ORIGINAL PAPER

An Experimental Study of Effect of High Temperature on the Permeability Evolution and Failure Response of Granite Under Triaxial Compression

Sheng-Qi Yang[1] · Wen-Ling Tian[1] · Derek Elsworth[2] · Jian-Guo Wang[1] · Li-Feng Fan[3]

Abstract

Granite is a viable host for deep nuclear waste disposal because its low permeability and high strength enable the stable and safe operation of the repository. We examined the evolution of the permeability and triaxial mechanical behaviour of granite after high-temperature treatment. First, the effect of the high temperature on the physical behaviour and permeability evolution of granite was analysed in detail. The mass, P-wave velocity, and thermal conductivity of granite decrease, but the volume increases with increasing temperature. The permeability of intact granite increases by four orders of magnitude as the cycled temperature increases from 25 to 800 °C. Subsequently, the effect of high temperature on the triaxial deformation and acoustic emission (AE) behaviour of granite was investigated. Under uniaxial compression at $T \leq 300$ °C, the stress decreases before the peak strength is reached, corresponding to a significant AE event, which is due to the development of multiple splitting tensile fractures along the loading direction. At $T \geq 450$ °C, AE event is observed once a minor stress is applied, which results from failure is controlled by thermally induced cracks. However, under triaxial compression, the temperature has little effect on the AE characteristics. The granite fails along the shear fracture plane, which becomes wider with increasing confining pressure. At $T \geq 600$ °C, it is easier to form intragranular cracks and the stress quickly decreases after the peak strength is reached. The shear plane is smoother under high confining pressure. Third, the effect of high temperature on the peak strength and crack damage threshold of granite was further analysed. Generally, under uniaxial compression, the peak strength and crack damage threshold first remain relatively constant at $T \leq 300$ °C, begin to decrease at $T = 450$ °C, and decrease more rapidly at $T = 600$ °C. The confining pressure notably reduces the effect of the temperature on the peak strength and crack damage threshold. Finally, the effect and mechanism of high temperature on the triaxial strength parameters of granite were further discussed. At $T \leq 300$ °C, thermally induced cracks are not notable and the temperature has little effect on the strength. At 450 °C $\leq T \leq 600$ °C, thermally induced cracks are more notable and the temperature has a significant effect on the strength behaviour. Because of the thermal stress released by thermal macrocrack formation, the continuous increase in the temperature has little impact on strength.

Keywords Granite · High temperature · Permeability · Peak strength · Triaxial compression

✉ Sheng-Qi Yang
  yangsqi@hotmail.com

1 State Key Laboratory for Geomechanics and Deep Underground Engineering, School of Mechanics and Civil Engineering, China University of Mining and Technology, Xuzhou 221116, People's Republic of China

2 Department of Energy and Mineral Engineering and G3 Center, Pennsylvania State University, 231 Hosler Building, University Park, PA, USA

3 College of Architecture and Civil Engineering, Beijing University of Technology, Beijing 100084, People's Republic of China

List of Symbols

A	Cross-sectional area of the specimen
L	Length of the specimen
μ	Dynamic viscosity of the fluid
P_1	Pressure on the upstream side
P_a	Standard atmospheric pressure at room temperature
K	Permeability of the specimen
Q	Mass flow of the gas at the downstream outlet
σ	Stress
σ_a	Axial stress
σ_m	Volumetric stress
σ_1	Maximum principal stress
σ_3	Confining pressure

p	Pore pressure
ε_1	Axial strain
ε_3	Circumferential strain
ε_v	Volumetric strain
T	Temperature
K_0	Initial permeability
K_u	Minimum permeability under elastic compression
α_m	A parameter in theoretical model of permeability
σ_S	Maximum supporting capacity (peak strength)
σ_c	Uniaxial compressive strength
σ_{cd}	Crack damage threshold
σ_{sd}	The sum of σ_{cd} and σ_3
E_S	Elastic modulus
ν	Poisson ratio of rock
Φ	Porosity
V_p	P-wave velocity
φ	Internal friction angle

1 Introduction

Granite is potentially an excellent medium for the disposal of high-level nuclear waste (HLW) because it exhibits a low native permeability and high integrity (Yang et al. 2017, 2018; Zhao et al. 2015). Beishan granite has been selected as a candidate for HLW disposal in China because of its low native permeability. However, the safe isolation of nuclear waste from human underground water is very important; thus, it is of great significance to study the permeability evolution of granite subjected to high temperature. During the decay of radionuclides, a large amount of heat is released, heating the rock mass around the emplaced place and causing damage (Chen et al. 2017a), and thus, it is valuable to find out the failure response of granite after high-temperature treatment under triaxial compression. Therefore, the permeability evolution and failure response of granite are important and must be known to assure the stable and safe operation of the HLW repository.

The physical characteristics and mechanical behaviour of granite after thermal treatment have been investigated for many years. High temperature can lead to the expansion of mineral grains, dehydration and chemical reaction of grains in the granite specimen, and transformation of the permeability evolution and failure behaviour. The physical characteristics of granite mainly refer to the colour, volume, mass, density, thermal conductivity coefficient, wave velocity, mineral composition, and distribution of microcracks. Thermal treatment can induce the initiation of microcracks in granite and other works, while the confining pressure can restrain the propagation and coalescence of microcracks (Wang et al. 1989). X-ray micro-CT (computed tomography) may be adopted to observe the distribution of microcracks in granite. The results show that granite achieves a maximum

anisotropy and heterogeneity at $T = 500$ °C (Fan et al. 2018). The propagation of microcracks with increasing temperature can be divided into four stages: $50 \,°C \leq T \leq 250 \,°C$, microcracks propagate stably; $250 \,°C \leq T \leq 350 \,°C$, crack formation accelerates; $300 \,°C \leq T \leq 350 \,°C$, cracks enter a transition stage; and $350 \,°C \leq T \leq 700 \,°C$, cracks enter a final development stage (Jiang et al. 2018). It has been reported that the heating–cooling process induces significant microcracking in granite, which are manifest as an increase in the porosity and gas permeability (Zhang et al. 2018). Optical microscopy and X-ray micro-CT, Yang et al. (2017) allow the interpretation of the mechanisms of high-temperature treatment impacting the mechanical properties of granite.

Real-time high-temperature tests and tests following high-temperature treatment are the two main methods that are used to investigate the influence of the high temperature on the failure and mechanical behaviours of granite. Real-time high-temperature tests are more approximate in representing response at the in situ stress state. Uniaxial and triaxial compression tests are two test methods that can be used to investigate the failure and mechanical behaviours of granite under real-time high temperature conditions. The highest temperature of ~ 1200 °C can be reached under uniaxial compression conditions (Shao et al. 2015). The uniaxial compressive strength (UCS), deformation, fracture, and acoustic emission (AE) characteristics of granite under real-time high temperature conditions have been previously investigated (Xu and Zhang 2018). Triaxial compression tests under real-time high-temperature conditions are based on the use of hydraulic fluid to provide the confining pressure and have difficulty in reaching temperatures > 600 °C (Zhao et al. 2017). Triaxial compression tests can be used to investigate the strength and shear parameters of granite under real-time high-temperature conditions. Combined with AE, damage analysis can be performed to define the strength response (Chen et al. 2018). Using the mechanical parameters obtained from triaxial compressive tests, the fracture characteristics anticipated around HLW repositories may then be simulated (Guo et al. 2018).

Tests following high-temperature treatment have been used for many years to investigate the influence of temperature on the mechanical behaviour of granite. Wang et al. (2017) compared the mechanical behaviour of granite under real-time high-temperature conditions both before and after thermal treatment. Their experimental results showed that real-time high-temperature conditions have a larger effect on the mechanical behaviour of granite than when viewing behaviour only after thermal treatment. However, the variation in the mechanical behaviour depending on the temperature of real-time high-temperature and post-thermal treatment conditions is similar. Therefore, tests of post-thermal treatment are commonly used to investigate the effect of the temperature on the mechanical behaviour of granite. The

degradation in the mechanical parameters as a result of thermal treatment is typically related to the mineral composition and microstructure of the granite (Chen et al. 2017b). Combining these observations of response with X-ray CT imaging shows that temperature has a significant effect on failure mode (Yang et al. 2017). Variations in the compressive strength, elastic modulus, tensile strength, and fracture toughness of granite have been analysed as functions of the temperature with four stages of behaviour identified. These stages are in the ranges of room temperature—200 °C, 200–400 °C, 400–600 °C, and > 600 °C, corresponding to undamaged, micro-damaged, secondarily damaged, and strongly damaged stages, respectively (Hu et al. 2018). High temperature also has a significant effect on peak strength, deformational characteristics, and failure modes of granite with pre-existing fissures (Huang et al. 2017). These properties are important for the evaluation of stability in rock engineering (Yang et al. 2019).

Because an HLW repository is underground, the deformation and failure of the surrounding rock mass are notably affected by in situ stresses. Therefore, it is crucially important to incorporate the roles of stress on failure and the resulting failure upon permeability evolution. In this study, the effect of high temperature on the mechanical characteristics and permeability evolution behaviour of granite was analysed in detail. Subsequently, the effect of high temperature on triaxial deformation and AE behaviour of granite was investigated and the peak strength and crack damage threshold were analysed. Finally, mechanisms responsible for these impacts of high temperature on the triaxial strength parameters of granite are discussed.

2 Experimental Methodology

2.1 Granite Material

As shown in Fig. 1, the granite used in this study was collected from Rizhao, Shandong Province, China. Based on X-ray diffraction (XRD), the granite comprises are quartz (11.12%), feldspar (59.85%), biotite (21.56%), amphibole (6%), chlorite (1.01%), and dolomite (0.46%). Figure 1 also shows the results of polarised light and optical microscopy of the granite. The granite has a crystalline structure with a connected porosity of 0.828% (Yang et al. 2017). Following the grain size terminology of Williams et al. (1954), the grain size of the granite ranges between 6 and 18 mm and is, thus, classified as a coarse-grained granite. At room temperature, the average density of the tested granite is 2594 kg/m³, and the P-wave velocity is approximately 4200 m/s. In this experiment, the cores of all specimens were obtained from the same block of material. The cores have a diameter of 50 mm and length of ~ 100 mm, resulting in a length: diameter ratio of 2:1 for the mechanical tests, which is in accordance with the International Society for Rock Mechanics (ISRM; Fairhurst and Hudson 1999) suggested method.

2.2 Permeability Testing System and Procedure

Before beginning the permeability tests, the granite specimens were first placed in a furnace and heated at a rate of 5 °C/min (Shao et al. 2015; Zhu et al. 2016). The predetermined temperature was kept constant for 2 h to ensure temperature homogeneity across the specimen. For the
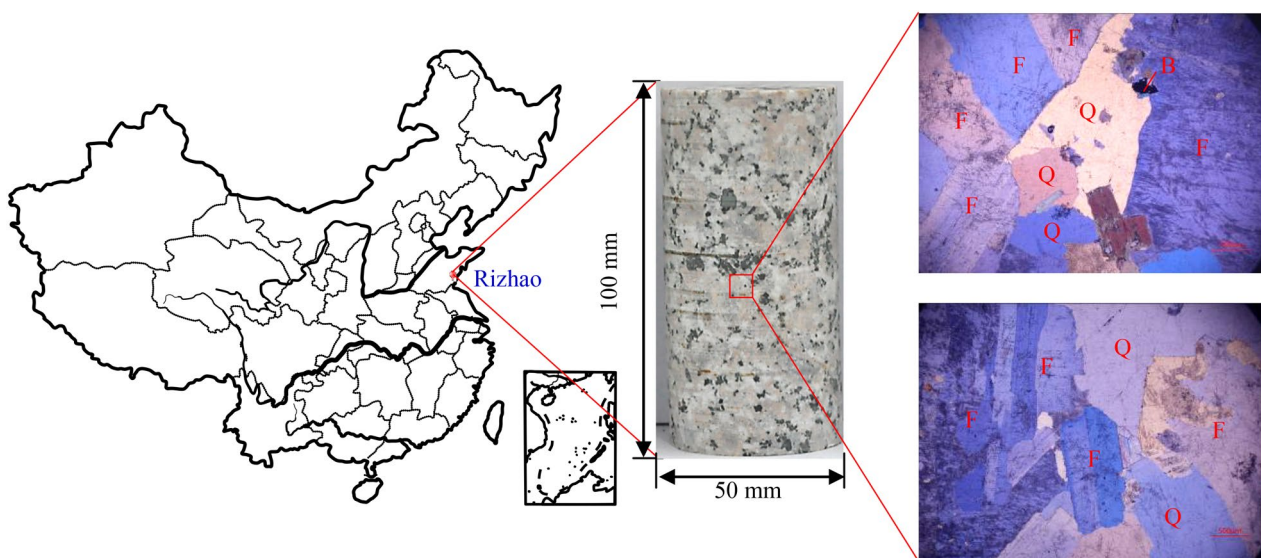
Fig. 1 Granite material with coarse-grained structure at room temperature in this study. *Q* quartz, *F* feldspar, *B* biotite

permeability tests, the target treatment temperatures were set to 25 °C, 100 °C, 200 °C, 300 °C, 400 °C, 500 °C, 600 °C, 700 °C, and 800 °C. After the thermal treatment, the heated specimens were left in the furnace to cool down to room temperature before measuring the permeability.

It is difficult to measure the coefficient of permeability of granite using steady-state liquid flow tests because the measurement time for one specimen is too long, ranging from several weeks to several months (Davy et al. 2007; Consenza and Ghoreychi 1999). Therefore, in this study, we used steady-state gas flow tests to measure the granite permeability.

The gas permeability test system (see Fig. 2) includes a gas pressure loading system, pressure control panel, gas pressure sensors, pressure loading system, and triaxial pressure chamber. The gas pressure loading system consists of a gas tank, flow pipes and valves in addition to a gas pumping system. Gas pressures may be elevated in the ranges 0–3 MPa to 0–40 MPa. The gas pressure sensors have three different scales to improve measurement accuracy. Furthermore, a high-precision pressure-controlled metering pump provides constant prescribed axial, lateral and triaxial stresses. Note that the maximum confining pressure of the test system is 60 MPa, which is smaller than the compressive strength of the granite tested in this experiment. The system can measure permeability to $> 10^{25}/m^2$ with this limitation resulting only from the enhance errors entrained in the excessive duration of the experiment.

The measurement of permeability under different triaxial stresses is described as follows. First, the cooled down specimen is imaged by high-magnification electron microscopy and its weight and dimensions are measured. For the permeability experiment, the cooled down specimen is placed into the triaxial pressure chamber and a small (0.1–0.2 MPa) axial stress is applied to ensure mating and sealing of the specimen ends with the platens. Subsequently, a confining pressure with a specified value is applied at a constant rate of 0.5 MPa/s. The confining pressure valve is then closed and the axial stress valve is opened to apply the designed axial stress on the specimen. Subsequently, the confining and axial stresses are kept constant, while a gas pressure is applied on the specimen using the pressure loading system. After each stress increment, the gas mass flow at the outlet end rapidly increases and then stabilises. The gas mass flow at the outlet side is recorded every minute. When the difference between the current and former values is lower than 2%, the value is regarded as the steady-state magnitude and the permeability under a certain triaxial stress can be calculated as:

$$Q = \frac{KAP_1^2}{2\mu L P_a}, \tag{1}$$

where A and L are the cross-sectional area and length of the specimen, respectively; μ is the dynamic viscosity of the fluid ($\mu \approx 1.8 \times 10^{-5}$ Pa s for pure nitrogen at room temperature under the applied pore pressure); P_1 is the pressure on the upstream side; P_a is the standard atmospheric pressure at room temperature; K is the permeability of the specimen; and Q is the mass flow of the gas at the downstream outlet.
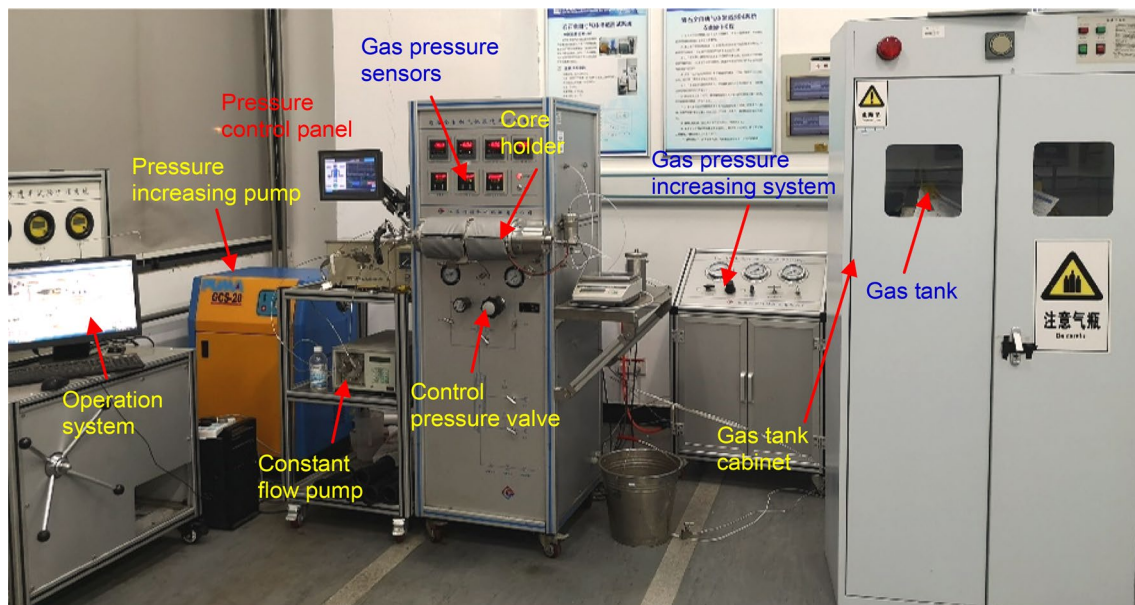
Fig. 2 Gas permeability test system developed by State Key Laboratory for Geomechanics and Deep Underground Engineering, China University of Mining and Technology

To ensure the stability and safety of deep nuclear waste disposal together with the influence of groundwater, it is important to identify the relationship between the permeability and effective stress of the rock. Therefore, a series of gas seepage tests was carried out on granite specimens with the same pore pressure under constant axial stress, confining pressure, and hydrostatic pressure. The compressive stress paths of the permeability tests of the granite specimens are shown in Fig. 3.

2.3 Mechanical Testing System and Procedure

Conventional triaxial compression was applied to the granite specimens using a GCTS RTX-4000 high-temperature and high-pressure rock triaxial testing system, as shown in Fig. 4a. The maximum axial loading capacity, maximum confining pressure, and maximum pore pressure were 4000 kN, 140 MPa, and 140 MPa, respectively. The axial and circumferential deformations were measured with an axial Linear Variable Differential Transducer (LVDT) with a maximum displacement range of 5 mm, as shown in Fig. 4b. During loading, the AE was monitored using a micro-II measuring system manufactured by the Physical Acoustic Corporation (PAC) and the amplitude threshold of the sensors was set to 60 dB.

The target treatment temperatures for the triaxial mechanical tests were set to 25 °C, 150 °C, 300 °C, 450 °C, 600 °C, and 750 °C. The heated granite specimens were left in the furnace to cool down to room temperature. After the thermal treatment, the granite was tested using a GCTS RTX-4000 high-temperature and high-pressure rock
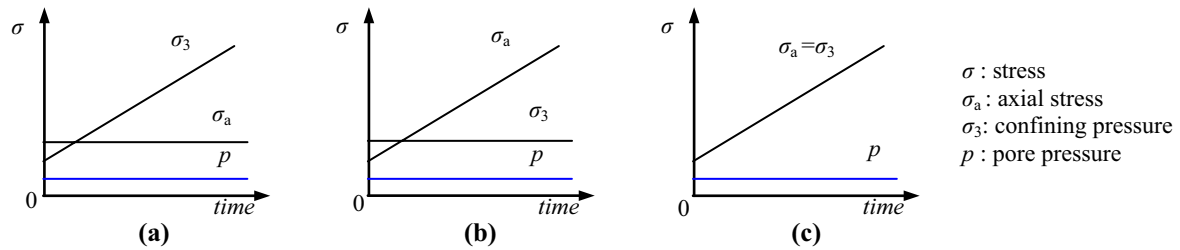
Fig. 3 Different compression stress paths in the permeability tests of granite specimens. **a** Constant axial stress and pore pressure; **b** constant confining pressure and pore pressure; **c** constant pore pressure but different hydrostatic pressure
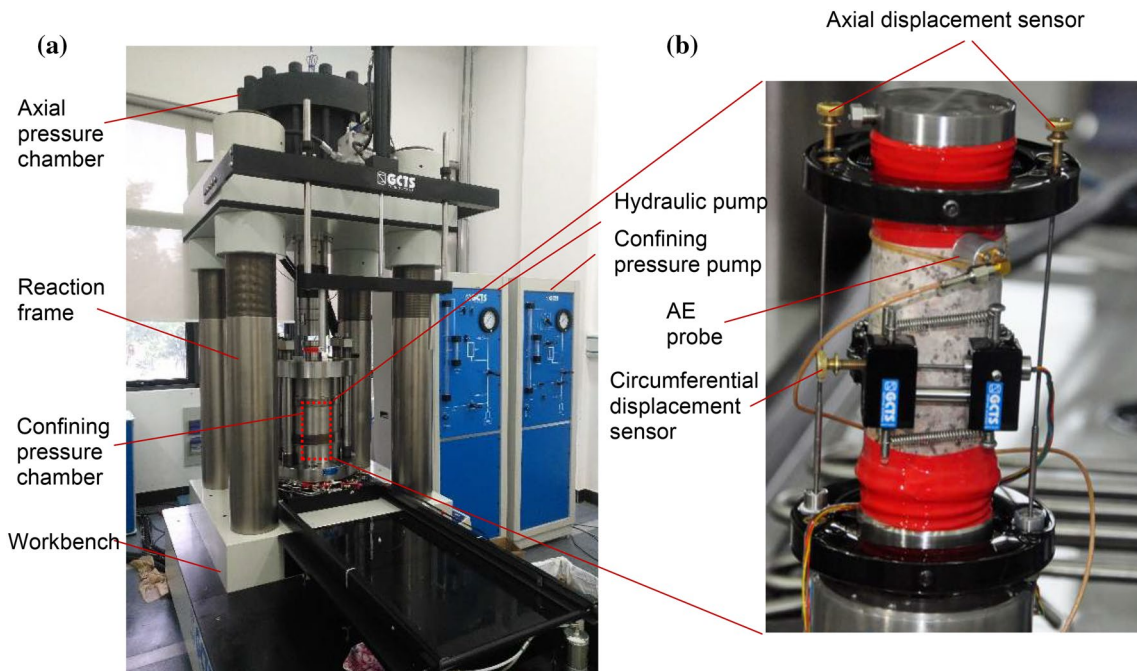
Fig. 4 RTX-4000 high-temperature and high-pressure triaxial rock testing system. **a** Overview of the testing system; and **b** detailed axial and lateral linear variable differential transducers

triaxial testing system with the confining pressure set to 0, 10, 20, 30, and 40 MPa, respectively.

The conventional triaxial experiments consisted of the following two steps: First, the confining pressure was increased to the desired value at a constant rate of 4.0 MPa/min to ensure that the specimen was under uniform hydrostatic stress. Deviatoric stress ($\sigma_1 - \sigma_3$) was then applied to the specimen at a constant axial displacement rate of 0.04 mm/min ($\sim 6.67 \times 10^{-6}$/s) until the post-peak failure stage was reached (in accordance with the method suggested by ISRM).

The Transient Plane Source (TPS) method introduced by Gustafsson (1991) and Log and Gustafsson (1995) was utilised to measure the thermal conductivity of the specimens. The hot disk sensor (a hot source and dynamic temperature sensor) was sandwiched between two specimens, as shown in Fig. 5. The hot disk sensor was first heated and then used to monitor the variation in the temperature (Zhao et al. 2016). This method has been widely applied to measure the thermal conductivity of rocks (Urquhart and Bauer 2015).

3 Effect of High Temperature on the Physical Behaviour and Permeability Evolution of Granite

3.1 Effect of High Temperature on the Physical Behaviour

We analyse the effect of high temperature on the physical behaviour of granite using the volume and mass variation rates of granite in response to changes in temperature, as shown in Fig. 6. The volume and mass variation rates are defined as the ratio between the changed and initial volumes and masses, respectively.

Figure 6a shows that the volume variation rate first increases at 150 °C and then remains relatively constant at 300 °C. This result is because the volume of the mineral grains in the granite increases with increasing temperature at $T \leq 300$ °C; but the residual strain of the mineral grains is smaller after cooling, resulting in an insignificant changes in the volume variation rate. At 450 °C, the volume variation rate starts to increase as a result of phase changes and

Fig. 5 The hot disk TPS-500 system
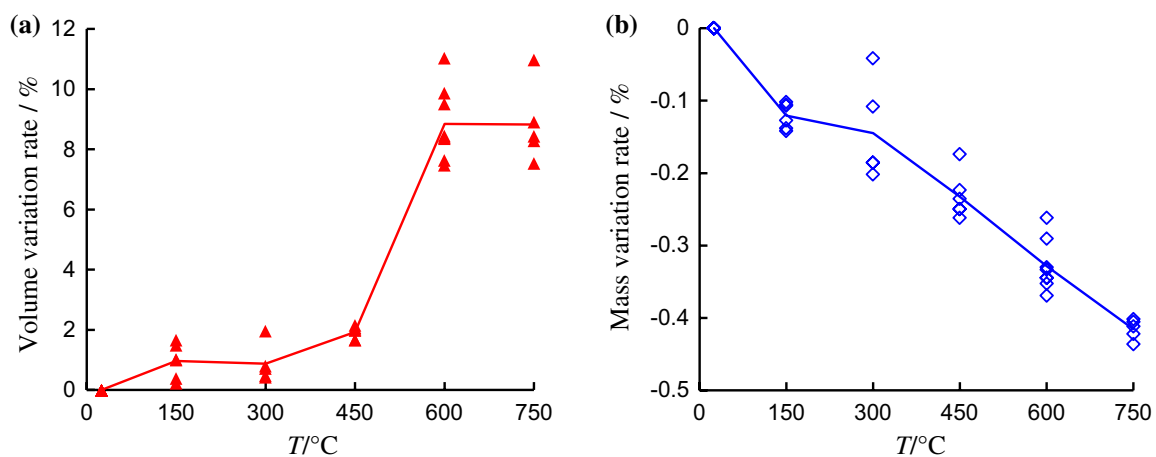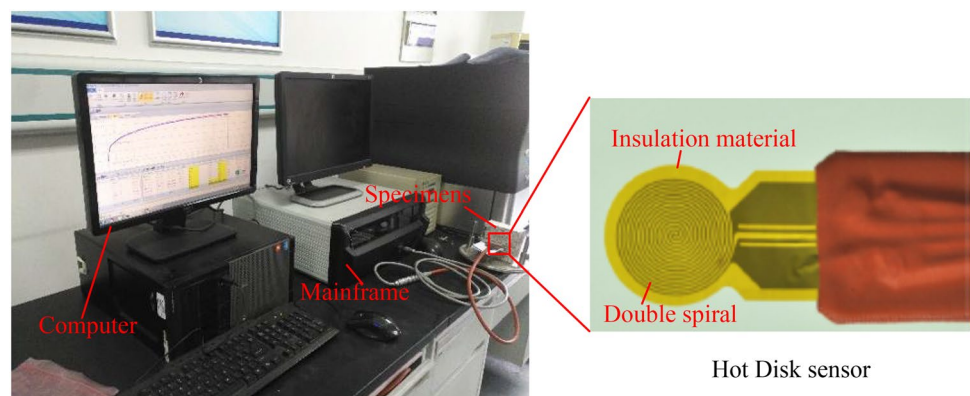
Fig. 6 Effect of high temperature on the volume and mass behaviour of granite in this research. (**a**) Volume variation rate; (**b**) Mass variation rate

the oxidation of biotite at 400 °C. Natural biotite exists in quasi-stable crystalline forms of 3 T and 1 M, whereas the stable crystal form of biotite is in a 2M1 state after heat treatment at temperatures above 400 °C. In addition, the Mg^{2+} in biotite oxidises during the heating (Sun 1987; Chen et al. 2017a):

$$K_2Mg_6^{2+}[Si_6Al_2O_{20}](OH)_4 + O_2$$
$$= K_2Mg_2^{2+}Mg_4^{3+}[Si_6Al_2O_{20}]O_4 + H_2O \uparrow$$

$$K_2Mg_6^{2+}[Si_6Al_2O_{20}](OH)_4 + O_2$$
$$= K_2Mg_2^{2+}Mg_4^{3+}[Si_6Al_2O_{20}]O_4 + 2H_2 \uparrow .$$
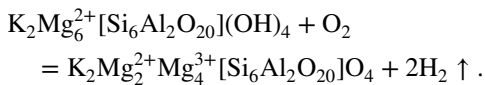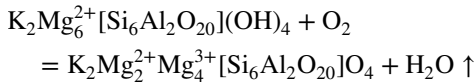
At 600 °C, the volume change rate of the granite specimen drastically increases. The quartz transforms from α phase to β phase. When the temperature exceeds 573 °C, the quartz grains will expand. However, the quartz retransforms from β phase to α phase as the temperature decreases to < 573 °C during cooling. The expansion of the quartz grains leads to the dislocation of mineral grains, initiation of cracks, and residual deformation above a temperature of 573 °C. At 750 °C, the volume variation rate remains relatively constant due to the formation of macrocracks at 600 °C and thermal stress release.

Heating can also lead to the dehydration of granite: at $25 °C \le T \le 100 °C$ as the absorbed water evaporates. At $100 °C \le T \le 300 °C$, the bound and crystal water escape; and at $300 °C \le T \le 400 °C$, the crystal and structural water escape (Sun et al. 2015). Therefore, the mass of the granite specimens decreases with an increase in temperature from 25 to 150 °C, as shown in Fig. 5b. However, at 300 °C, the mass decrease slows down because the amount of bounded and crystal water in the granite specimen is relatively low. As a result of the oxidation of biotite and the escape of

crystal and structural water, the mass of the granite quickly decreases again at 450 °C. At 600 °C, the mass of granite also decreases quickly because of the phase transformation of quartz and fragments separating from the specimen. At 750 °C, the mass continuously decreases. This may be due to continuous separation of fragments—suggested by the observation that the values of the volume variation rate are generally larger than the values of the mass variation rate.

The variation in the thermal conductivity caused by thermal damage is related to heat dissipation and stability of the nuclear waste repository. Knowledge of the thermal conductivity as a function of the temperature is critical for the stable operation of the repository (Sundberg and Hellström 2009; Zhao et al. 2016). The change in thermal conductivity with temperature was measured using a TPS-500 system (Fig. 5), as shown in Fig. 7a. At $T \le 300 °C$, the thermal conductivity decreases almost linearly with increasing temperature; at 450 °C, the thermal conductivity decreases with increasing temperature again approximately linear; and at 600 °C, the thermal conductivity notably decreases, indicating that the large amount of microcracks caused by the quartz phase transition leads to a notable decrease in the thermal conductivity of granite. However, as the temperature increases from 600 to 750 °C, fewer new thermal cracks form and the thermal conductivity remains relatively constant. The thermal conductivity at $T = 750 °C$ is 1.22 W/mK, which is 50% of the room temperature value of 2.53 W/mK, indicating that high temperature has a significant effect on the thermal conductivity of granite.

Figure 7b shows the effect of high temperature on the P-wave velocity of the granite, providing a potential method to evaluate the variation in thermal damage. Figure 7b shows that the P-wave velocity linearly decreases with increasing temperature at $T \le 450 °C$; at $T = 600 °C$,
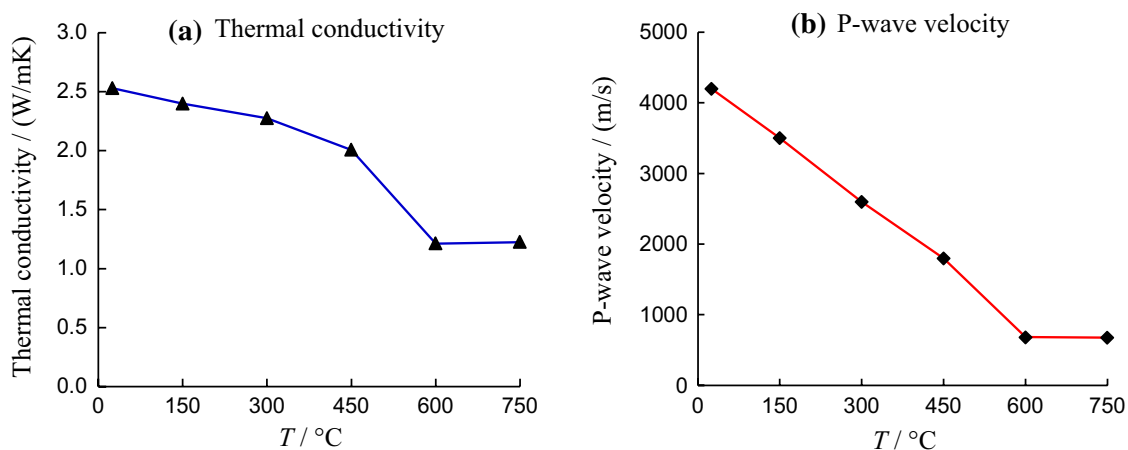
Fig. 7 Effect of high temperature on thermal conductivity and P-wave velocity of granite in this research. **a** Thermal conductivity; **b** P-wave velocity

the P-wave velocity rapidly decreases, indicating significant damage to the granite specimen under the influence of high temperature. At 750 °C, the P-wave velocity remains essentially unchanged over the range 600–750 °C with the increase in temperature resulting in little new damage. These trends in behaviour with temperature are similar to those previously observed for Beishan granite (Zhao et al. 2018).

Heating can induce thermal microcracks in granite, leading to changes in the physical and mechanical behaviour of granite specimens. Figure 8 shows the microstructure of granite after thermal treatment obtained from optical microscopy. At $T \leq 300$ °C, very few initial microcracks are observed and the mineral grains are tightly cemented. At 450 °C, intergranular cracks can be observed, which means that the microstructure is weakened by thermal stress. Figures 6 and 7 show that the temperature of 450 °C represents an inflection point with respect to changes in volume and thermal conductivity. At 600 °C, an intergranular network of cracks forms around each grain, which is due to the phase transformation of quartz that causes the polygonal grains to become isolated. In addition, several intragranular cracks form. At 750 °C, the distribution of the microcracks is similar to that at 600 °C, but the resulting microcracks are wider.

3.2 Effect of High Temperature on Permeability Evolution Under Triaxial Compression

A series of permeability measurements with various gas pressures was completed with the permeability calculated using Eq. (1). The mass flow rate of the gas is proportional to the gas pressure enabling permeability to be accurately obtained.

Figure 9a shows the relationship between the gas pressure and mass flow rate (Q–P_1 curve) after the specimens were treated at different temperatures. Figure 9a shows that the curve steepens with increasing temperature, which means that the permeability increases notably. Figure 9b shows that the permeability varies with increasing temperature because the hydrostatic stress significantly influences the permeability of rocks. The volumetric stress (σ_m) is plotted in Fig. 9b. The figure shows that the temperature has a significant effect on the permeability at a volumetric stress of 50 MPa. Figure 9b shows that the permeability increases from 10^{-18} to 10^{-14} (0.001–10 mD) when the temperature increases from 25 to 800 °C. In other words, the permeability is 10,000 times as large as the initial value when the temperature increases from 25 to 800 °C. Furthermore, note that the permeability of the granite increases insignificantly as the temperature increases from 25 to 300 °C. The permeability coefficient of granite then increases slightly when the temperature increases from 300 to 500 °C, but increases rapidly from 500 to 800 °C.

Figure 10 shows the permeability evolution of granite after different high-temperature treatments. In Fig. 10, three different loading paths, as shown in Fig. 3, are predesignated. These represent, respectively, an axial stress increase under constant confining pressure, a confining pressure increases under constant axial stress, and an increase in axial stress and confining stress at the same rate (hydrostatic pressure). The maximum axial stress and confining pressure is limited to 60 MPa by the experimental apparatus. Importantly, this is significantly smaller than

(a) $T = 25$°C **(b)** $T = 150$°C **(c)** $T = 300$°C **(d)** $T = 450$°C

(e) $T = 600$°C **(f)** $T = 600$°C **(g)** $T = 750$°C **(h)** $T = 750$°C
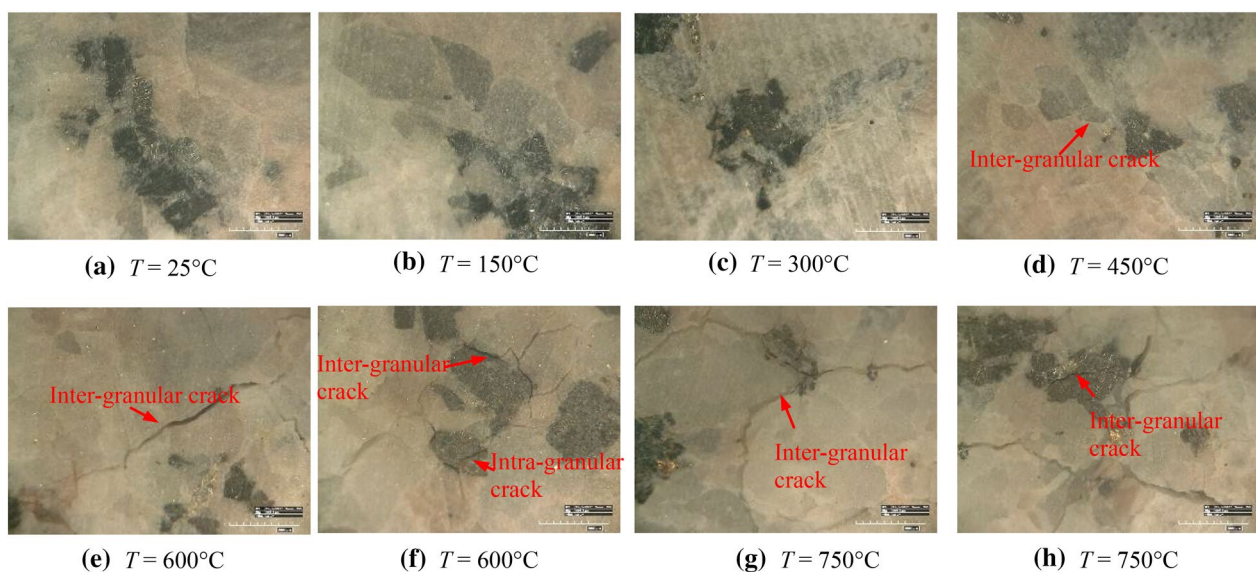
Fig. 8 Micro-structure of granite after thermal treatment obtained by optical microscopy (×50)
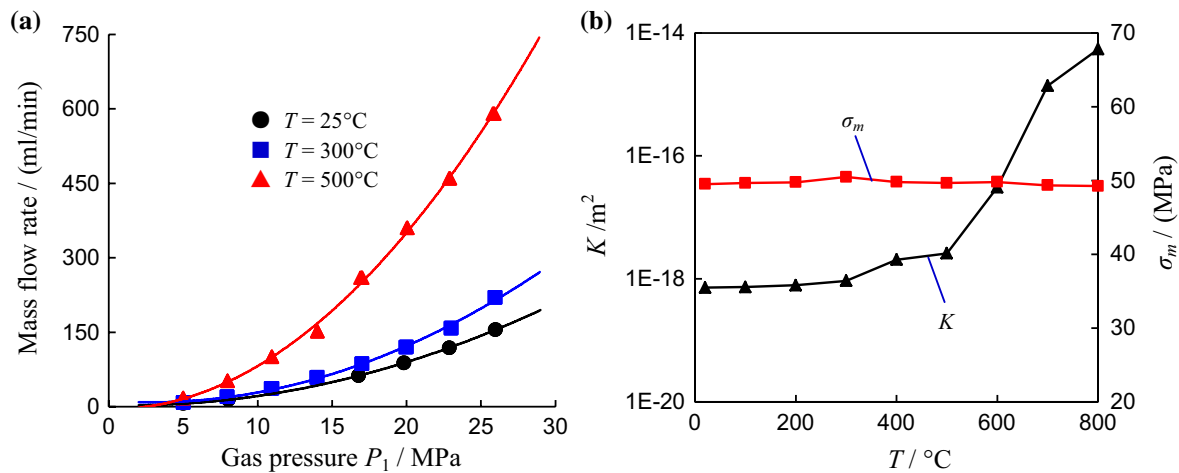
Fig. 9 Effect of high temperature on mass flow rate and permeability of granite specimen. **a** Relationship between mass flow rate and gas pressure; **b** relationship between permeability and temperature

the UCS according to the results of uniaxial compression experiments on granite (Yang et al. 2017). Accordingly, the granite specimen experiences elastic compression only.

Figure 10 shows that the permeability of granite decreases with increasing axial and confining pressure, while the confining pressure (σ_3) has a larger influence than the axial stress (σ_a) in the range of 10–50 MPa. Taking the experimental result for 25 °C as an example, when the axial stress increases from 10.13 to 49.04 MPa ($\sigma_3 = 10$ MPa), the permeability coefficient of granite decreases from 0.0031 to 0.0026 mD, while the permeability of granite sharply decreases from 0.00426 mD (4.26×10^{-18} m^2) to 0.000668 mD (6.68×10^{-19} m^2) with the increase in the confining pressure from 9.86 to 49.3 MPa ($\sigma_a = 10$ MPa). This may be related to the difference between the directions of the permeability measurement and axial stress. The permeability of granite under different hydrostatic pressures is also shown in Fig. 10. The influence of hydrostatic pressure on the permeability varies with temperature.

To analyse the effect of the volumetric stress (σ_m) on the permeability of granite, the following theoretical model was constructed in this study:

$$K = (K_0 - K_u) \exp(-\alpha_m \sigma_m) + K_u, \qquad (2)$$

where K_0 is the initial permeability; K_u is the minimum permeability under elastic compression; and α_m is a model parameter, which is related to the deformation modulus.

Figure 11 shows typical effect of volumetric stress on the permeability of granite specimens at $T = 25$ and 800 °C. From Fig. 11, we can see that the permeability of the granite specimens decreases exponentially with increasing volumetric stress, while the deviatoric stress is zero. The theoretical curves calculated using Eq. (2) were compared with the

experimental results. The theoretical curves agree very well with the experimental results. With increasing volumetric stress, the permeability of the granite specimens first rapidly decreases and then gradually stabilises.

The initial permeability (K_0) is that at zero compressive stress. With increasing volumetric stress, the permeability gradually decreases to a constant value under elastic compression, which is regarded as the ultimate permeability of rock. Figure 12a shows that the initial and ultimate permeabilities of granite have similar correlations with temperature. With increasing temperature, the initial and ultimate permeabilities simultaneously increase. A notable exponential relationship can be observed between the initial permeability and temperature as well as the ultimate permeability.

Based on the theoretical curves shown in Fig. 11, we can obtain the variation in the parameter α_m with temperature, as shown in Fig. 12b. Figure 12b shows that the α_m value increases as the temperature increases from 25 to 500 °C, but it decreases sharply at temperatures above 500 °C. The physical meaning of parameter α_m is that the volumetric strain under compression increases notably with the increase in parameter α_m (Xu and Yang 2019), which also means that the bulk modulus is inversely proportional to α_m.

4 Effect of High Temperature on Triaxial Deformation and AE Behaviour of Granite

4.1 Triaxial Stress–Strain Curves of Granite After Different High-Temperature Treatments

Figure 13 shows triaxial deviatoric stress–axial strain and circumferential strain curves of granite after different high-temperature treatments. The triaxial stress–strain curve of
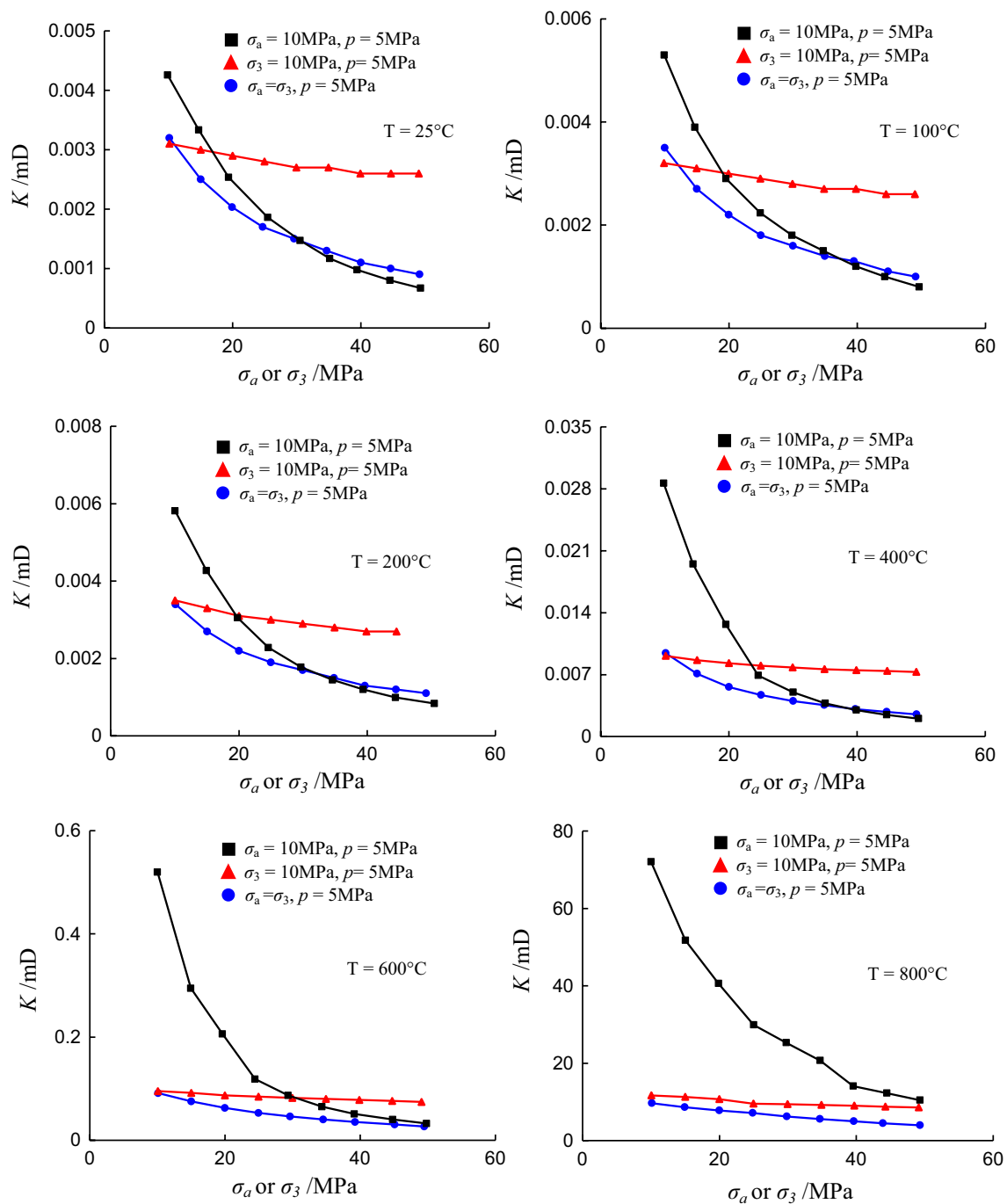
Fig. 10 Effect of effective stress on permeability of granite specimens after different high temperatures

granite can be divided into five stages: (I) initial pore and fissure closure stage, (II) elastic deformation stage, (III) plastic deformation stage, (IV) post-peak failure stage, and (V) residual strength stage.

(I) Initial pore and fissure closure stage: The axial strain of granite increases quickly, while the axial deviatoric stress increases slowly. The deviatoric stress–axial strain curve is concave. The initial pore and fissure closure stage

becomes less notable with increasing confining pressure due to the closure of the micro-fissures and micro-pores. Note that, at the same confining pressure, more micro-fissures and micro-pores in the specimens initiated by thermal damage can be observed with increasing temperature and thus, initial pore and fissure closure stage becomes more notable.

$K = (7.148\exp(-0.059\sigma_m) + 0.269) \times 10^{-18}$

$R^2 = 0.99$

(a) $T = 25°C$

$K = (12.518\exp(-0.064\sigma_m) + 0.531) \times 10^{-14}$

$R^2 = 0.99$

(b) $T = 800°C$
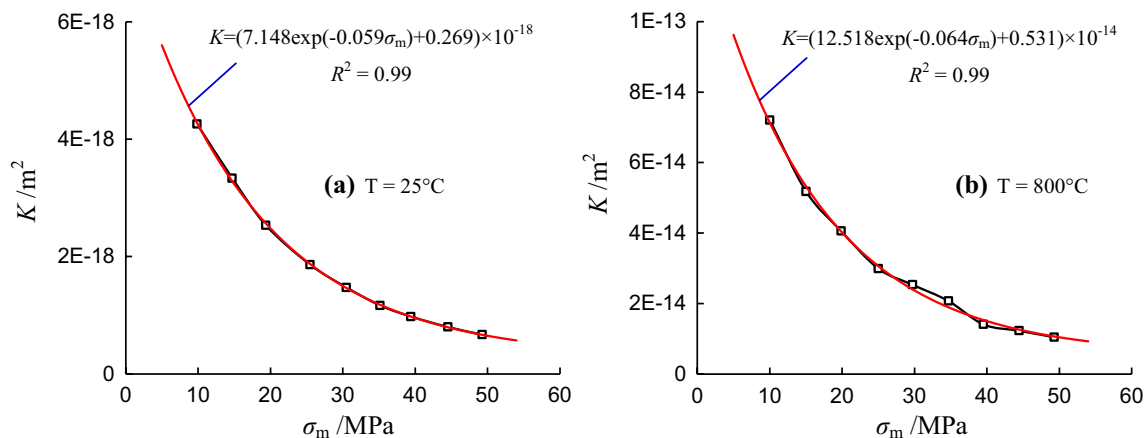
Fig. 11 Typical effect of volumetric stress on permeability of granite specimens at $T = 25$ and 800 °C

- ■ Initial permeability ($\sigma_m = 0$)
- ▲ Hydrostatic compression ($\sigma_m = 50$MPa)
- ● Ultimate permeability

(a)

(b) The variation of parameter α_m of with temperature
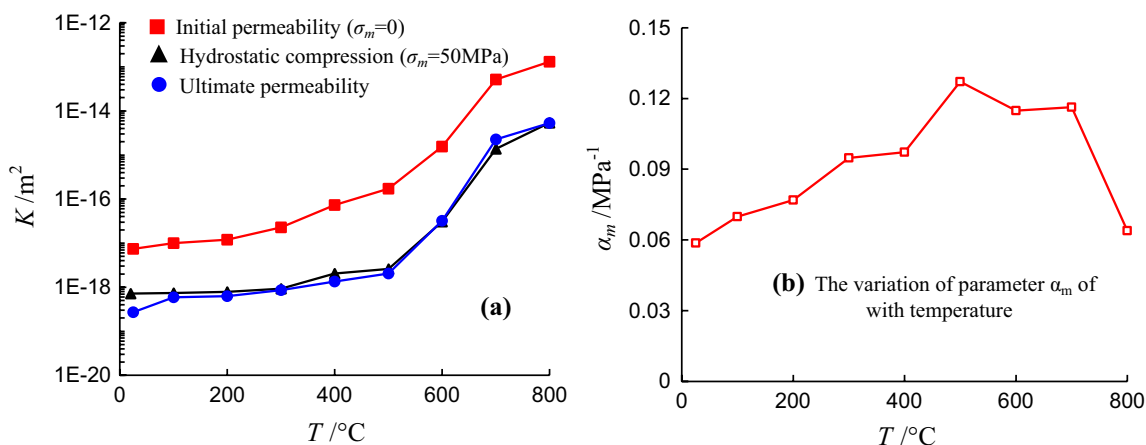
Fig. 12 Effect of temperature on the permeability and the variation of parameter α_m of granite specimen. **a** The variation of initial and ultimate permeability under elastic compression with temperature; **b** the variation of parameter α_m with temperature

(II) Elastic deformation stage: The deviatoric stress increases linearly with increasing axial and circumferential strain. The slope between the deviatoric stress and axial strain increases with increasing confining pressure and becomes more sensitive to the confining pressure after undergoing higher-temperature treatment. After high-temperature treatment, the structure of granite specimens becomes looser due to thermal damage. The confining pressure restrains the displacement and enhances the friction among grains and the slope becomes more sensitive to the confining pressure under the condition of higher temperature.

(III) Plastic deformation stage: The slope between the deviatoric stress and axial strain decreases with increasing axial strain, and the circumferential strain increases nonlinearly. Under uniaxial compression, the stress concentration leads to local failure in granite specimens because they lose their ability to resist the deformation. The slope continues

to decrease before the peak strength is reached, which corresponds to the rapid increase in the circumferential strain. With increasing temperature, more thermal micro-cracks are initiated and the bearing structure of granite specimen is damaged. Therefore, the ability to store strain energy in granite specimens decreases and the mineral grains have more spaces to adjust. When local stress failure occurs, less strain energy is released and fewer cracks propagate. Thus, the decrease of slope is not notable. Under the influence of the confining pressure, more adjustment abilities are observed among mineral grains and it is difficult to produce the stress concentration nearby the grains. Therefore, a stress drop cannot be observed in the stress–strain curve of the granite under the confining pressure.

(IV) Post-peak failure stage: The increase of microcrack initiation, propagation, and coalescence are observed during the loading process. Therefore, macrocracks form and the stress decreases quickly with increasing axial strain.
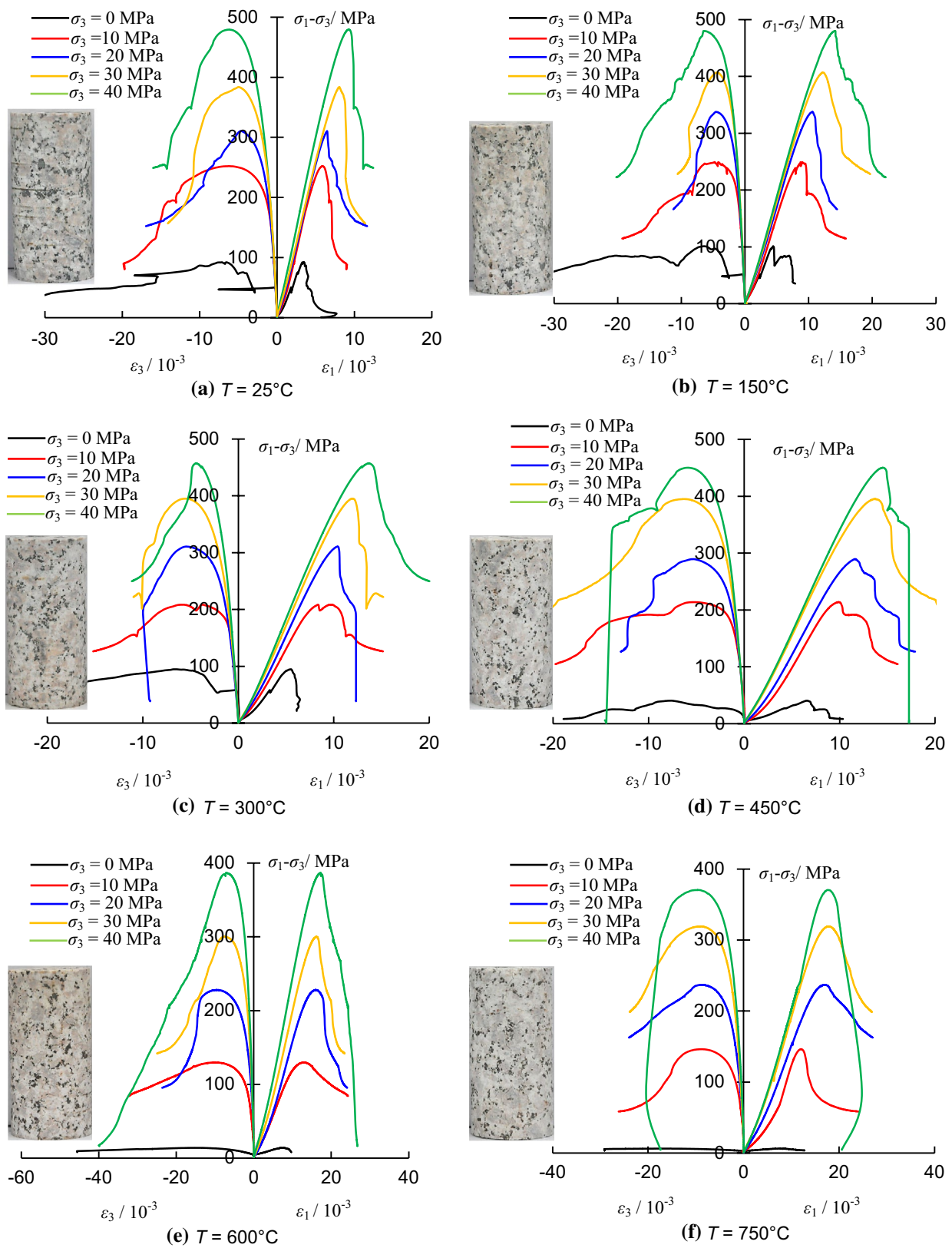
Fig. 13 Deviatoric stress–axial strain and circumferential strain curves of granite specimens after high-temperature treatment under different confining pressures

At $T \leq 450$ °C, the granite specimens experience more local damage under uniaxial compression; the deviatoric stress–strain curves, thus, show more stress drops and the granite specimens fail slowly. At $T \geq 600$ °C, less strain energy is stored in the granite specimen and the deviatoric stress decreases gradually after reaching the peak strength. Under the influence of confining pressure, the granite specimens fail generally along the shear fracture plane. The tested granite specimens have coarse-grained structures and the intragranular failure involves more stress than intergranular failure. Therefore, the cracks can propagate more easily along intergranular fracture planes than intragranular fracture planes. At $T \leq 450$ °C, the deviatoric stress decreases gradually with increasing axial strain due to intergranular shear plane propagation. At $T \geq 600$ °C, the peak strength of the granite specimens decreases due to heat-induced intragranular cracks. At a higher confining pressure ($\sigma_3 = 40$ MPa), intragranular cracks form more easily with the decrease of axial stress, the shear plane is smoother, and the stress decreases dynamically, as shown in Fig. 13e, f.

(V) Residual strength stage: under the influence of confining pressure, interlocking and friction forces exist between the mineral grains of the granite specimens. Therefore, the deviatoric stress remains relatively constant with continuous loading after the post-peak failure stage. The interlocking and friction forces increase with increasing confining pressure, which also leads to the increase in the residual strength with increasing confining pressure. At $T \geq 600$ °C and a higher confining pressure ($\sigma_3 = 40$ MPa), the shear plane is smoother, which leads to a lower residual strength of the granite specimen.

The evolution of the volumetric strain (ε_v) after high-temperature treatment and for different confining pressures is shown in Fig. 14. The parameter ε_v refers to the volumetric strain, which is calculated from the sum of the axial strain (ε_1) and twice the radial strain (ε_3; i.e. $\varepsilon_v = \varepsilon_1 + 2\varepsilon_3$). The volumetric strain is characterised by an initial phase of compaction-dominated behaviour followed by a phase of dilatancy-dominated behaviour, as shown in Fig. 15c. After point A, the compaction is in direct competition with dilatancy (although the specimen is still in a state of net compaction). Eventually, the rates of compaction and dilatancy become equal at point B, resulting in an inflection point in the volumetric strain curve. The crack damage threshold (σ_{cd}) of the specimen (Wong et al. 1997; Fairhurst and Hudson 1999; Heap et al. 2009; Yang et al. 2015) is defined as the corresponding axial deviatoric stress at which the volumetric deformation of the specimen switches from compaction dominated to dilatancy dominated. As the stress further increases, more microcracking occurs and the granite specimen continues to dilate. The volumetric strain of the granite specimen eventually returns to zero strain (Point C) and then continues to increase until the specimen fails.

At $T \leq 450$ °C, the potential for volume shrinkage during subsequent loading is small due to the closure of partial cracks under the confining pressure. Therefore, under the same axial stress, the amount of shrinkage of the specimen decreases with increasing confining pressure before the crack damage threshold is reached. The corresponding volume strain is also smaller. Under uniaxial compression, the local expansion of the cracks causes a sudden volume expansion, which is due to the axial splitting of the specimen under uniaxial compression. Due to the restrained confining pressure, the specimen expands rapidly following damage. Under the confining pressure, the volume expansion of the specimen is restricted. The volume expansion rate of the specimen decreases as the confining pressure increases. At $T \geq 600$ °C, the crystal grains are liable to slip during the compression because the bearing structure of the specimen is broken such that the specimen expands in the beginning of uniaxial compression. The thermal cracks in the specimen close under the influence of the confining pressure, the friction between the crystal grains increases, and the bearing capacity of the specimen rapidly increases. High confining pressure also causes a decrease in the volumetric shrinkage potential of the specimen. Therefore, the volumetric compression rate of the specimen decreases with increasing confining pressure before the damage threshold is reached. Similarly, the confining pressure limits the volume expansion of the specimen. After the crack damage threshold is reached, the volume expansion rate of the specimen decreases with increasing confining pressure.

4.2 Effect of High Temperature on Deformation Parameters Under Triaxial Compression

Figure 15a, b, respectively, presents the variation of the elastic modulus (E_S) of granite depending on the temperature and confining pressure. The elastic modulus is defined by the average slope of the approximately straight portion (i.e. from the elastic initial value to the elastic limit) of the axial deviatoric stress–axial strain curve before the peak strength is reached.

From Fig. 15a, it can be seen that the elastic modulus of granite under uniaxial compression slightly increases when the temperature increases from 25 to 150 °C and slowly decreases when the temperature increases from 150 to 300 °C. This elastic modulus then quickly decreases as the temperature increases from 300 to 600 °C and then remains relatively constant when the temperature increases continuously to 750 °C. Note that the elastic modulus of granite under uniaxial compression increases from 25 to 150 °C for the following reasons. The absorbed and bound water in the specimen evaporates and escapes, which increases the friction forces between the crystal grains. Additively, thermal residual deformation, the bond between the crystal grains
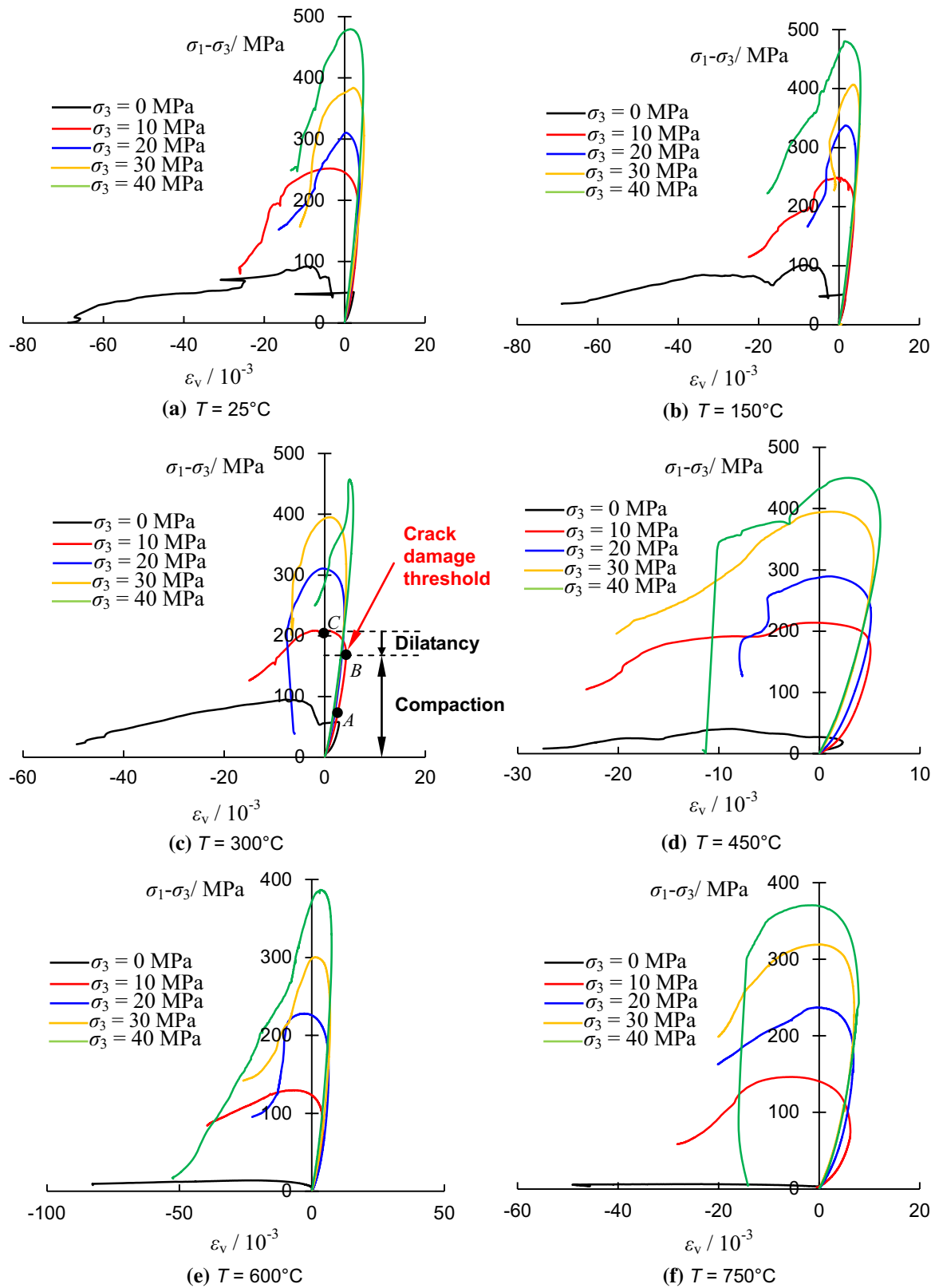
Fig. 14 Deviatoric stress–volume strain curves of granite specimens after high-temperature treatment under different confining pressures
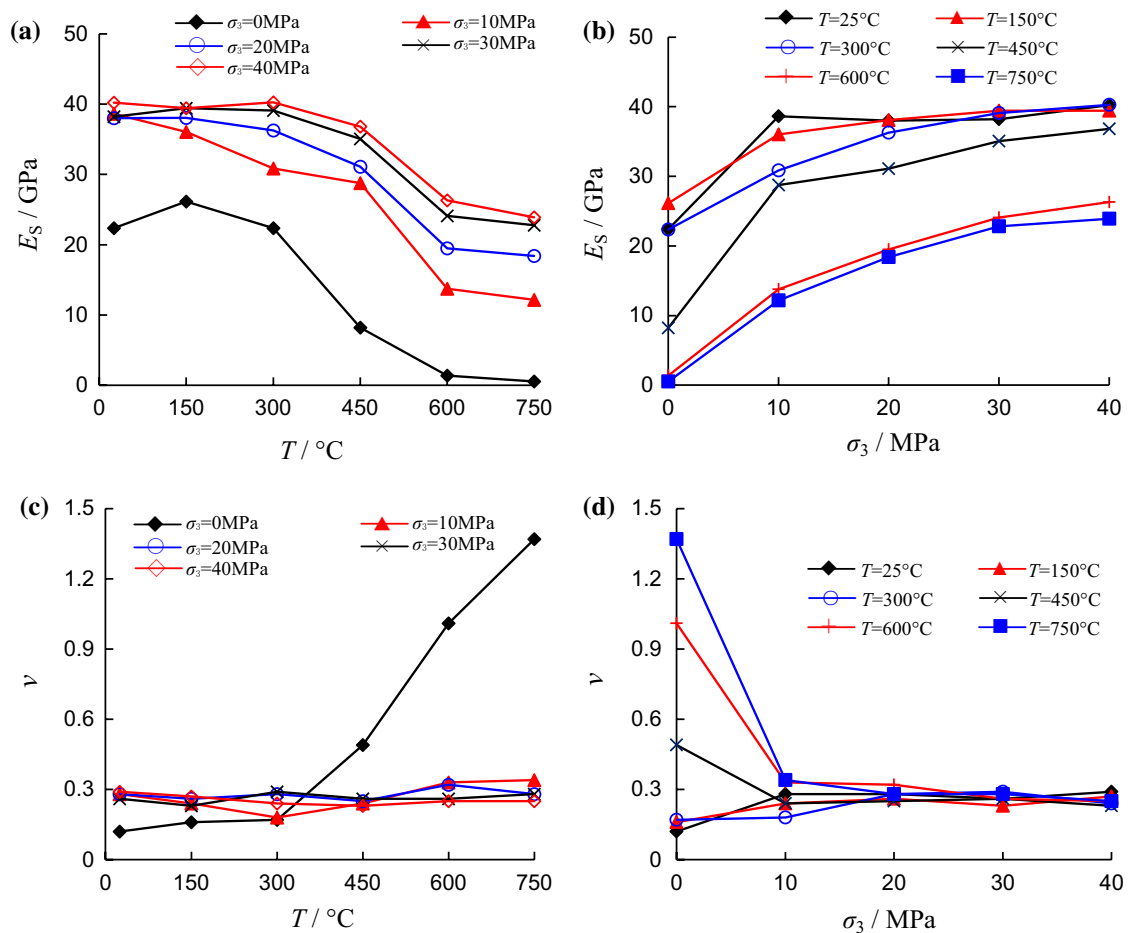
Fig. 15 Deformation parameters of granite specimens after high-temperature treatment with temperature and confining pressure. **a** Variation of elastic modulus with temperature; **b** variation of elastic modulus with confining pressure; **c** variation of Poisson ratio with temperature; **d** variation of Poisson ratio with confining pressure

becomes higher. These two effects are additive and result in an increase in the elastic modulus of the granite under uniaxial compression as the temperature increases from 25 to 150 °C. Thermal cracks continue to appear as the temperature increases from 150 to 600 °C, resulting in a decrease in the elastic modulus of the specimen under uniaxial compression. However, the increase in the confining pressure leads to the closure of some of the thermal cracks such that the elastic modulus decreases with decreasing temperature at the same confining pressure. When the temperature increases from 600 to 750 °C, the thermal stress is released due to the occurrence of through-going macroscopic cracks and the formation of later cracks becomes difficult. Therefore, the elastic modulus changes insignificantly.

From Fig. 15b, it can be seen that the elastic modulus of the granite quickly increases when σ_3 increases from 0 to 10 MPa at 25 °C and 150 °C. Subsequently, the E_S of the granite remains relatively constant with continuously increasing confining pressure. At 300 °C and 450 °C, the elastic modulus

of granite also quickly increases as σ_3 increases from 0 to 10 MPa, but only slowly increases with the confining pressure when σ_3 is greater than 10 MPa. At 600 °C and 750 °C, the elastic modulus continuously and nonlinearly increases with increasing confining pressure. Based on the above-mentioned analysis, the elastic modulus of the granite rapidly increases as the confining pressure increases from 0 to 10 MPa, which is independent of the temperature. With the continuous increase in the confining pressure from 10 to 40 MPa, the rate of increase in the elastic modulus also increases with increasing temperature. At $T = 25$ °C and 150 °C, almost no microcracks can be observed in the granite specimens, except for the initial pores. Therefore, the increase in the confining pressure from 10 to 40 MPa cannot result in the closure of microcracks and pores. However, at $T = 600$ °C and 750 °C, more thermal cracks are induced and the potential for microcrack and pore closure is large. With increasing confining pressure, the microcracks and pores continue to close and the frictional

force greatly increases. This leads to the continuous increase in the elastic modulus.

Figure 15c, d shows the variation in the Poisson ratio (ν) of the granite specimens after high-temperature treatment at different confining pressures. The Poisson ratio is the average of the absolute ratios of the circumferential strain and axial strain in the range of 30–70% of the triaxial compressive strength. Figure 15c shows that the Poisson ratio under uniaxial compression first increases gradually when the temperature increases from 25 to 300 °C and then rapidly increases when the temperature increases from 300 to 750 °C. Under the influence of the confining pressure, the temperature has almost no effect on the Poisson ratio of granite. Following high-temperature treatment, the granite specimens contain more microcracks and the mineral grains in the granite specimens rotate more easily. Therefore, the granite specimens more easily expand in the circumferential direction under uniaxial compression. However, the confining pressure restrains the rotation of the mineral grains and thus the temperature only has a small effect on Poisson ratio under triaxial compression. Figure 15d depicts the variation in Poisson ratio of the granite specimens depending on the confining pressure. From Fig. 15d, we can see that the confining pressure also has only a small effect on Poisson ratio at $T \leq 300$ °C. At $T \geq 450$ °C, the Poisson ratio significantly decreases when the confining pressure is applied and then remains relatively constant with continuously increasing confining pressure. This means that thermal cracks are initiated in the specimen at 450 °C and the mineral grains rotate more easily. The confining pressure can restrain the rotation of the grains and thus, the Poisson ratio quickly decreases under the increased confining pressure. However, while the confining pressure can restrain the grain rotation, closure of thermally induced cracks can also occur, leading to a decrease in the adjustment space of mineral grains. Under axial loading, the expansion in the circumferential direction is easier than in axial direction. Therefore, the Poisson ratio of granite remains relatively constant when the confining pressure increases.

4.3 Effect of High Temperature on the AE and Failure Behaviour Under Triaxial Compression

Figures 16 and 17 show the typical AE characteristics of granite specimens after high-temperature treatment under uniaxial and triaxial ($\sigma_3 = 30$ MPa) compression. The temperature has a significant effect on the AE characteristics. The AE and AAE represent the acoustic emission and accumulated acoustic emission, respectively. Under uniaxial compression at $T \leq 300$ °C, a stress decrease can be observed before the peak strength is reached, which corresponds to a significant AE event. This means that local damage occurs before the peak strength is reached under uniaxial compression. However, at $T \geq 450$ °C, AE can be observed when axial compression is applied because more thermal cracks are induced and the grains immediately begin to adjust. Under triaxial compression, the temperature has little effect on the AE characteristics. However, at $T \geq 600$ °C, intragranular cracks more easily form and the stress quickly decreases after the peak strength is reached. The AE does not increase after the peak strength is reached.

Figure 18 presents the ultimate failure modes of granite after thermal treatment under triaxial compression. The granite specimens fail in an axial splitting tensile mode under uniaxial compression, while they fail in a shear mode under triaxial compression. Under uniaxial compression at $T \leq 450$ °C, the splitting tensile cracks are numerous and almost parallel to the loading direction although few bifurcate. The multiple splitting events correspond to multiple stress drops during loading. At $T \geq 600$ °C, more thermal macrocracks are induced in the granite specimens and the ultimate failure mode is controlled by these thermally induced macrocracks. Tensile cracks are densely distributed in the specimen and not completely parallel to the loading direction. During loading, the thermally induced macrocracks coalesce. The cracks slowly propagate and the stress–strain curves show increased ductility.

Under triaxial compression, the failure mode of the granite specimens at room temperature transforms from a single shear plane to rhombohedral shear plane with increasing confining pressure, and the shear fracture plane widens with increasing confining pressure. At $T = 150$ °C and 300 °C, the widening of the cracks is more notable. At $T = 450$ °C, the shear plane widens with increasing confining pressure, while two parallel shear planes exist at $\sigma_3 = 40$ MPa. Because intergranular fractures form more easily than intragranular cracks and also interlocking and frictional forces increase with increasing confining pressure, grains close to the shear plane exert a greater influence on the grains neighbouring when the shear plane forms—resulting in a widening of the shear plane. At $T \geq 600$ °C, the grains weaken and thermally induced and intragranular cracks more easily form under high shear stress. Therefore, the shear plane is smoother under a high confining pressure ($\sigma_3 = 40$ MPa), which corresponds to a sudden stress decrease after the peak strength is reached.
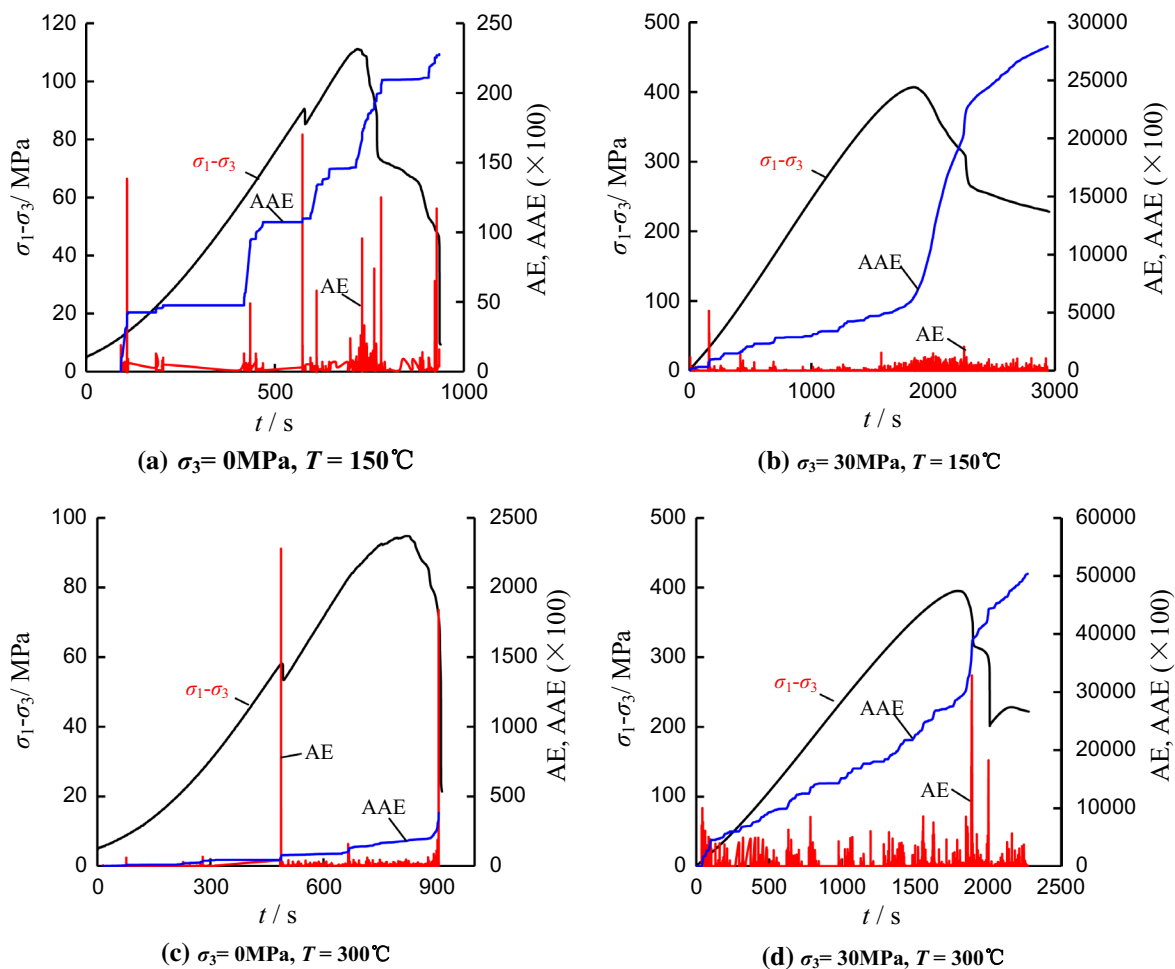
Fig. 16 Typical AE characteristic of granite specimens after high-temperature treatment ($T = 150$ °C and 300 °C) under uniaxial and triaxial ($\sigma_3 = 30$ MPa) compression

5 Effect of High Temperature on Strength Behaviour of Granite Under Triaxial Compression

5.1 Effect of High Temperature on Peak Strength Behaviour Under Triaxial Compression

Figure 19a shows the variation in the peak strength of granite under triaxial compression as a function of temperature. At $T \leq 300$ °C, absorbed, bound, and crystal water escape, but smaller residual strain and thermally induced microcracks occur. At 300 °C $\leq T \leq 500$ °C, the crystal and structural water escape and Mg^{2+} in biotite oxidises, resulting in several heating-induced microcracks. At $T = 573$ °C, more thermal microcracks are initiated and macrocracks form due to the phase transformation of quartz. Because of the formation of macrocracks, thermal stress is released and the continuous increase in the temperature does not lead to the formation of more microcracks. Therefore, the peak strength of the granite remains relatively constant under uniaxial compression at $T \leq 300$ °C. The peak strength of granite quickly decreases at 300 °C $\leq T \leq 600$ °C. Subsequently, the peak strength stabilises at 600 °C $\leq T \leq 750$ °C. With increasing confining pressure, the interlocking and frictional forces between the grains increase, which can lead to an increase in the peak strength. At the same time, the confining pressure can lead to the closure of heat-induced cracks. The peak strength, therefore, remains relatively constant at $T \leq 450$ °C. At $T = 600$ °C, more cracks are induced by heating and the peak strength of granite notably decreases. The effect of the temperature on the peak strength of granite decreases with increasing confining pressure.

Figure 19b depicts the variation in the peak strength of granite after different high-temperature treatments with increasing confining pressure. The peak strength of the granite increases with increasing confining pressure, regardless of the temperature. Note that the peak strength nonlinearly increases with increasing confining pressure. Furthermore,
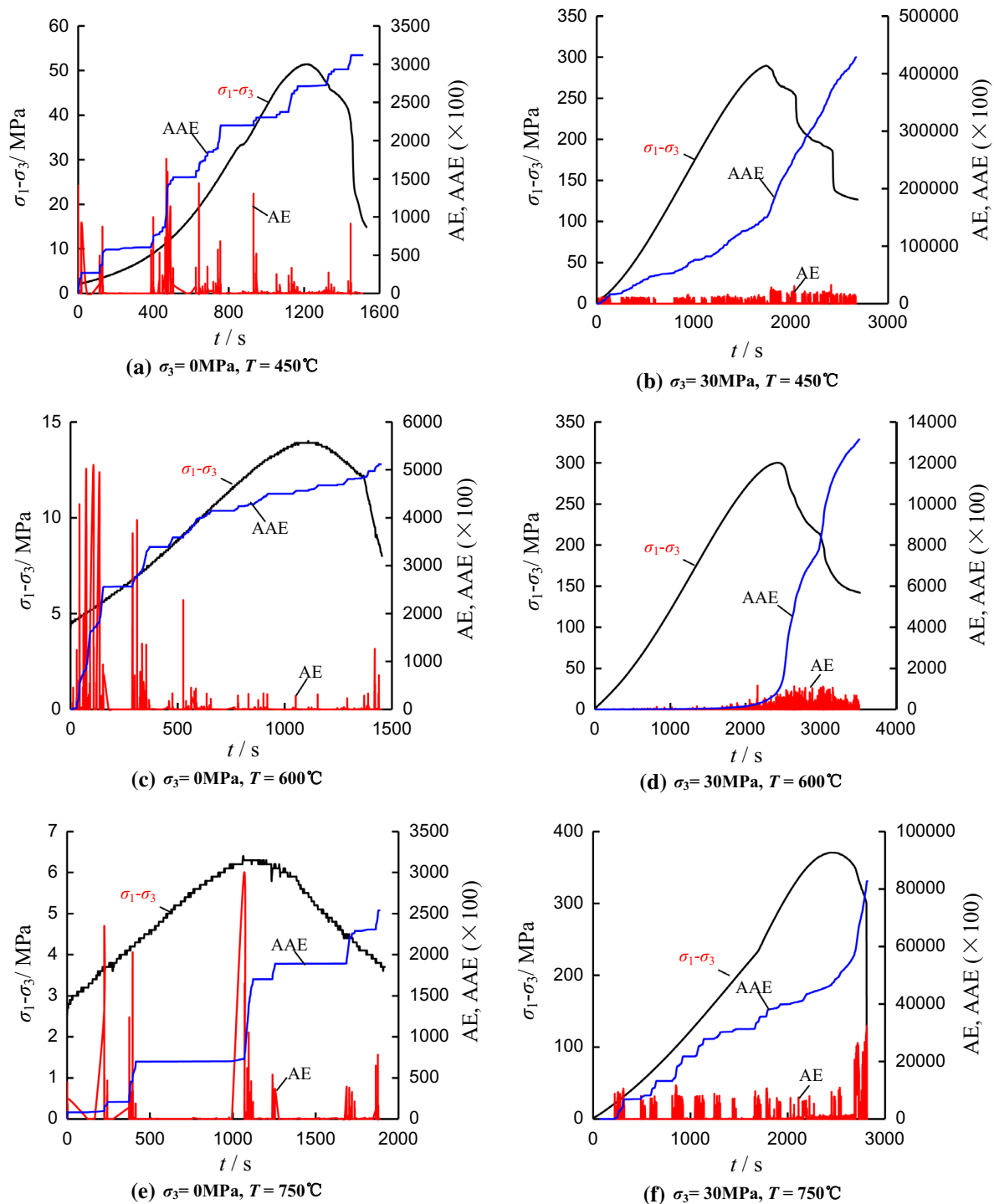
Fig. 17 Typical AE characteristic of granite specimens after high-temperature treatment ($T = 450$ °C, 600 °C and 750 °C) under uniaxial and triaxial ($\sigma_3 = 30$ MPa) compression

the nonlinearity becomes more pronounced with increasing temperature. The amount of thermally induced cracks increases with increasing temperature and the confining pressure can induce the closure of these cracks. Therefore, if the amount of thermally induced cracks is larger, the increase in the peak strength becomes more notable after the confining pressure is applied. If the uniaxial compressive strength is not used for the regression, the peak strength of the granite increases near linearly with increasing confining pressure.

(a) $T = 25°C$

(b) $T = 300°C$

(c) $T = 600°C$

Fig. 18 Ultimate failure mode of granite specimen after high-temperature treatments under different confining pressures
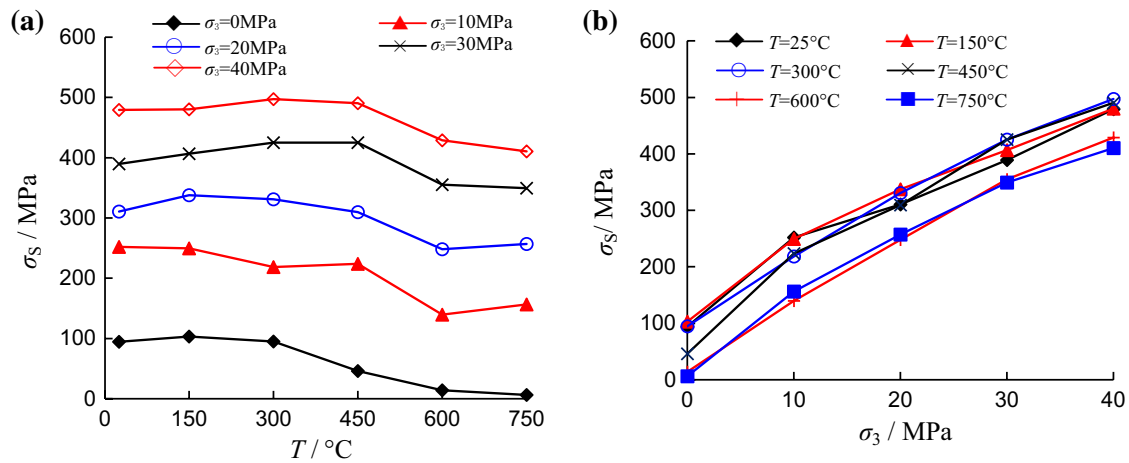
Fig. 19 Variation of the peak strength of granite specimens after high-temperature treatment with temperature and confining pressure. **a** Variation with temperature, **b** variation with confining pressure

5.2 Effect of High Temperature on the Crack Damage Threshold Under Triaxial Compression

Figure 20a presents the crack damage threshold under triaxial compression with increasing temperature. Similar to the peak strength, the crack damage threshold under uniaxial compression remains relatively constant at $T \leq 300$ °C and quickly decreases when the temperature increases from 300 to 600 °C. At $T \geq 600$ °C, the bearing structure of the granite is damaged, the granite specimens immediately expand under uniaxial loading, and the crack damage threshold is close to zero

Confining pressure can restrain the initiation of cracks; thus, the crack damage threshold increases with increasing confining pressure. Figure 20b shows that the crack damage threshold increases nonlinearly with increasing confining

pressure, similar to the peak strength. The crack damage threshold also increases linearly with the confining pressure, except for that under uniaxial compression. The confining pressure can result in the closure of thermally induced cracks and reduction of the stress concentration at the tips of cracks. Therefore, the propagation of thermally induced cracks is restrained. Furthermore, the confining pressure can change the directions of crack initiation and propagation. The failure mode of granite specimens can transform from tensile splitting to shear fracture. The crack damage threshold of granite quickly increases with increasing confining pressure. The confining pressure reduces the stress concentration but also restrains the crack propagation, whereas it does not notably change the crack initiation and propagation directions. Therefore, the crack damage threshold linearly increases with increasing confining pressure.
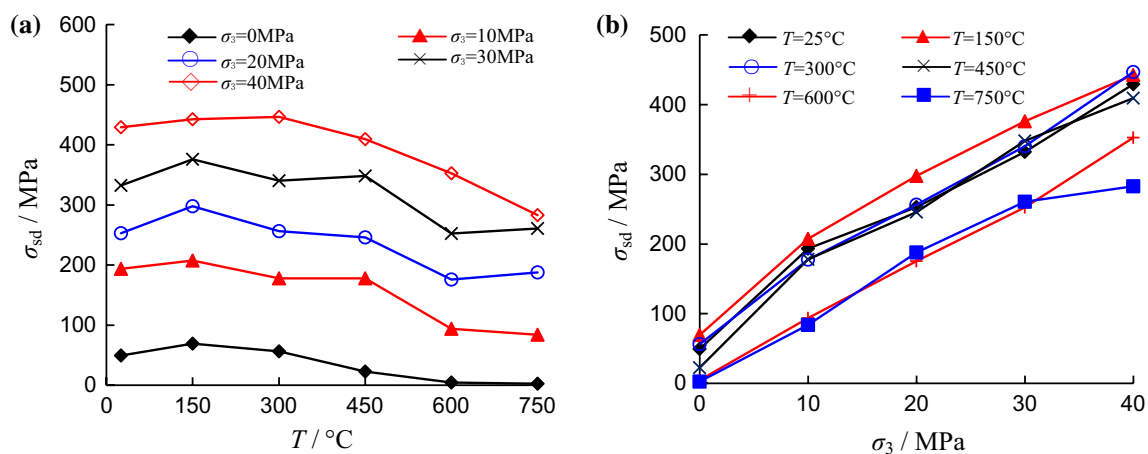
Fig. 20 Variation of the crack damage threshold of granite specimens after high-temperature treatment with temperature and confining pressure. **a** Variation with temperature, **b** variation with confining pressure

Note that the peak strength and crack damage threshold of granite slightly increase when the temperature increases from 25 to 150 °C. In theory, cracks are induced by heating and the strength decreases. At $T = 150$ °C, grain expansion may not induce thermal cracks and absorbed, bound, and crystal water escape, which leads to an increase in the frictional resistance between the grains. Based on direct shear tests, Mitchell et al. (2013) investigated the variation in the frictional coefficient depending on the temperature, as shown in Fig. 21a. The frictional coefficient increases linearly with temperature. Therefore, the peak strength and crack damage threshold increase at 150 °C.

Figures 19a and 20a show that the confining pressure can reduce the effect of temperature excursions on the peak strength and crack damage threshold. To quantify the effect of temperature on the peak strength and damage threshold, the ratio between the mean squared error and average value of the peak strength and crack damage threshold after the same temperature treatment was introduced. Figure 21b shows that the ratio is maximal. This means that the temperature has the greatest effects on the peak strength and crack damage threshold. At $\sigma_3 = 10$ MPa, the ratio quickly decreases, suggesting that the application of the confining pressure notably reduces the effect of the temperature on the peak strength and crack damage threshold. However, the ratio slowly decreases with increasing confining pressure, suggesting that an increase in the confining pressure only slightly decreases the effect of the temperature on the peak strength and crack damage threshold.

5.3 Effect of High Temperature on Hoek–Brown Criterion Strength Parameters

To illustrate the nonlinear response of the peak strength and crack damage threshold of granite to the confining pressure, the Hoek–Brown criterion (Hoek and Brown 1980; Hoek

1990) can be used. It describes the relationship between the peak strength, crack damage threshold, and confining pressure. The Hoek–Brown criterion can be expressed as:

$$\sigma_S = \sigma_3 + \sigma_c \left(m \frac{\sigma_3}{\sigma_c} + s \right)^{0.5}, \tag{3}$$

where σ_c is the uniaxial compressive strength and m and s are basic parameters representing the rock, which vary depending on the rock type. The parameter m reflects the weakness of the rock. The bigger the $-m$ coefficient, the stronger the rock. The parameter s reflects the extent of pre-existing (or evolving) fractures and ranges from 0 to 1 with unity representing intact rock.

To describe the strength and fracture of granite after thermal treatment, σ_c is set to the uniaxial compressive strength of granite at room temperature. When s is larger than 1, s is set to 1, and when s is smaller than 0, s is set to 0. Based on the regression of the peak strength and crack damage threshold under different confining pressures, s and m values of the granite specimens after different temperature treatments are obtained. Figure 22a shows that the parameter s is obtained from the peak strength and is relatively constant with an increase in temperature from 25 to 150 °C. However, s quickly decreases to 0 with the increase in the temperature from 150 to 600 °C. Subsequently, it remains zero when the temperature increases to 750 °C. The parameter s is obtained from the crack damage threshold and increases slightly with an increase in the temperature from 25 to 150 °C. The s parameter obtained from the crack damage threshold quickly decreases to zero with an increase in the temperature from 150 to 600 °C. Finally, this remains zero when the temperature increases to 750 °C. This analysis shows that almost no thermal cracks are induced in the specimens at $T \leq 300$ °C, but thermally induced cracks propagate quickly at 300 °C $\leq T \leq$ 600 °C. When the temperature increases from
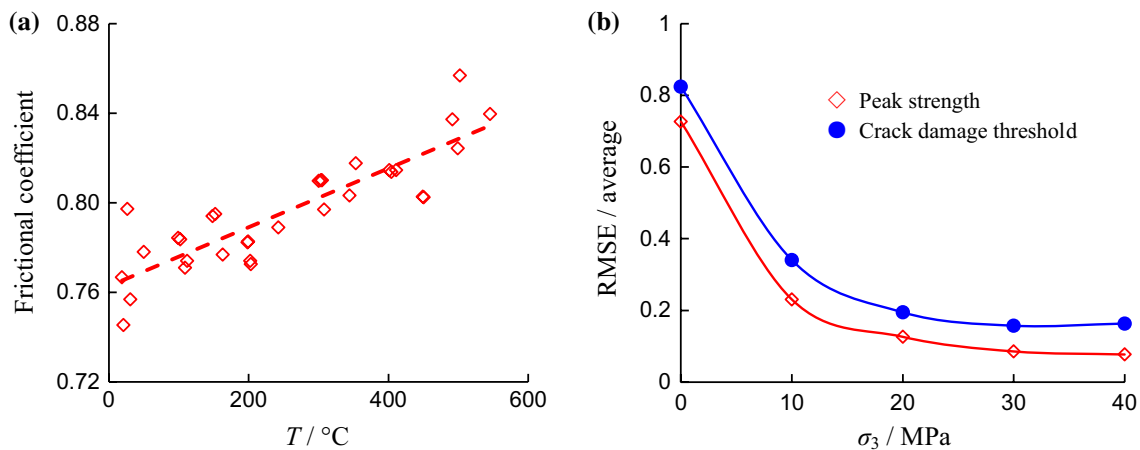
Fig. 21 Frictional coefficient of granite with the temperature and ratio between RMSE and average with the confining pressure
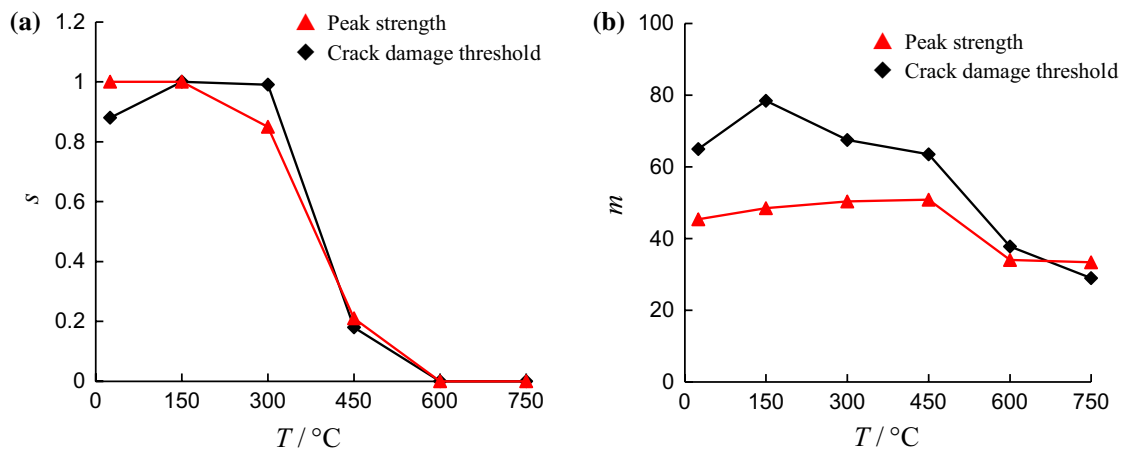
Fig. 22 Variation of the Hoek–Brown parameters of the peak strength and crack damage threshold of granite specimens after high-temperature treatment with temperature. **a** *s*, **b** *m*

600 to 750 °C, it is difficult for thermally induced cracks to propagate due to the formation of macrocracks.

Figure 22b shows the variation in the parameter *m* obtained from the peak strength and crack damage threshold depending on the temperature. The parameter *m* obtained from the peak strength first increases with the increase in the temperature from 25 to 450 °C and then quickly decreases with the increase in the temperature from 450 to 600 °C. Finally, it remains relatively constant with an increase in the temperature to 750 °C. The *m* parameter obtained from the crack damage threshold first increases with the increase in the temperature from 25 to 150 °C and then decreases with increasing temperature. Based on this analysis, the specimen becomes stronger at 150 °C. However, the *m* parameter obtained from the peak strength increases when the temperature increases from 150 to 450 °C, while its crack damage threshold decreases. This indicates that cracks are more easily induced after thermal treatment and the ductility and frictional coefficient of the grains increase. This leads to a decrease in the stronger and weakness extent of the crack damage threshold, while the stronger and weakness extent of the peak strength increases. When the temperature increases from 600 to 750 °C, the stronger and weakness extent of the peak strength and crack damage threshold remain relatively constant.

5.4 Mechanistic Control of High-Temperature Effects on Strength and Permeability

The strength and elastic modulus of rocks generally decrease with increasing temperature due to thermally induced cracks. However, the experimental results show that the peak strength and crack damage threshold increase slightly at 150 °C. The origin of the thermally induced strengthening of sandstone at temperatures below 500 °C may be related to

strain hardening based on localised plasticity development and to the transformations of goethite to hematite and/or smectite to illite at more modest temperatures on the order of 300 °C (Ranjith et al. 2012). Based on XRD results, Chen et al. (2017a) reported that the mineral composition of granite insignificantly changes after thermal treatment; however, the crystalline forms of the minerals change. Based on SEM observations of granite after thermal treatment, the microcrack closure due to thermal expansion improves the granite structure, which leads to an increase in its strength (Huang et al. 2017). However, SEM only scans the granite specimens locally and thus is not representative for the overall characteristics of the granite samples. The variation in the porosity (Φ) and P-wave velocity (V_p) of granite after thermal treatment is known to depend on the temperature, as shown in Fig. 23a. The results show that the porosity slowly increases with increasing temperature at $T \leq 400$ °C and then quickly increases at $T \geq 400$ °C. The rate of decrease of V_p is the ratio between the V_p decrease by thermal treatment to the V_p of granite specimens at room temperature. The rate of decrease of V_p is reflects the damage level of granite based on thermal treatment. Figure 23b shows that the V_p decreasing rate almost linearly increases with increasing temperature. Figure 23 shows that the amount of thermally induced cracks increases with increasing temperature, which contrasts with the hypothesis that microcrack closure due to thermal expansion improves the structure of the granite (Huang et al. 2017).

To verify that the amount of thermally induced cracking increases with increasing temperature, the permeability (K) of the granite after different high-temperature treatments was measured under different effective stresses. Figure 11 shows that the permeability of the granite decreases nonlinearly with increasing effective stress, regardless of the temperature. At the same effective stress, the permeability
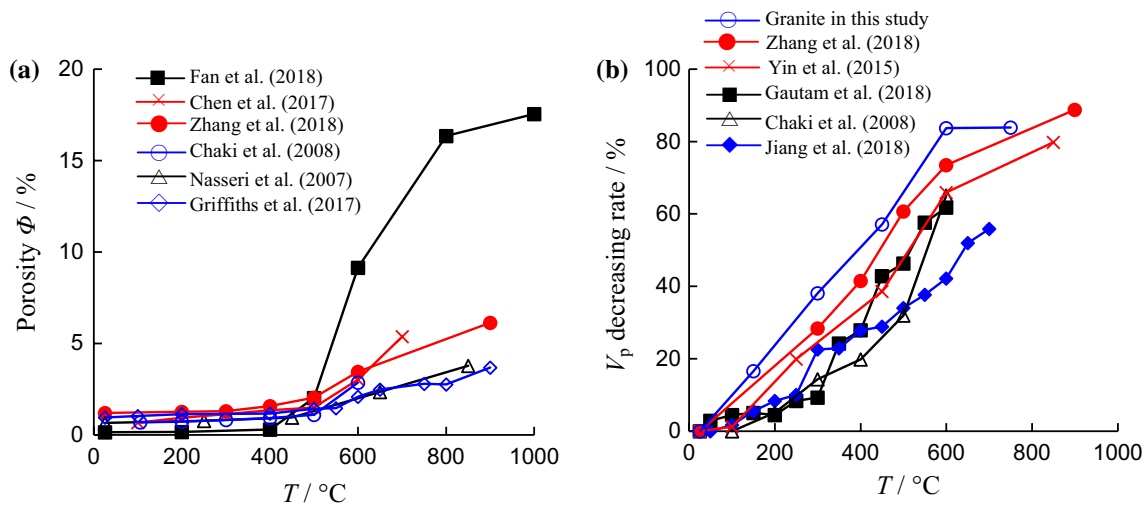
Fig. 23 Porosity and V_p decreasing rate with temperature. **a** Porosity, **b** V_p decreasing rate

of the granite increases with increasing temperature. The relationship between the permeability and porosity is shown in Eq. (2) (McKee et al. 1988). The porosity of granite increases with increasing temperature according to the ratio.

$$K \propto \frac{\phi^3}{(1-\phi)^2}. \qquad (4)$$

As explained in the previous section, the increase in the strength at 150 °C may be due to the increase in the frictional coefficient with increasing temperature (Mitchell et al. 2013). Therefore, a Mohr–Coulomb criterion was used to investigate the effect of the confining pressure on the peak strength and crack damage threshold of granite and thus the internal friction angle (φ) can be obtained. Figure 24 shows that the internal frictional angle of the granite obtained from the peak strength and crack damage threshold first increases with increasing temperature at $T \leq 450$ °C. The figure also shows that the strength increase at $T = 150$ °C may be due to the increase in the frictional coefficient with increasing temperature.

6 Conclusions

Granite is an excellent potential host for HLW repositories because of its low permeability and significant integrity. Based on experimental results for permeability evolution and failure response of granite subjected to thermal cycling, the following conclusions can be drawn.

1. The effect of high temperature on the physical behaviour of granite was analysed using the volume variation rate, mass variation rate, P-wave velocity, and thermal con-
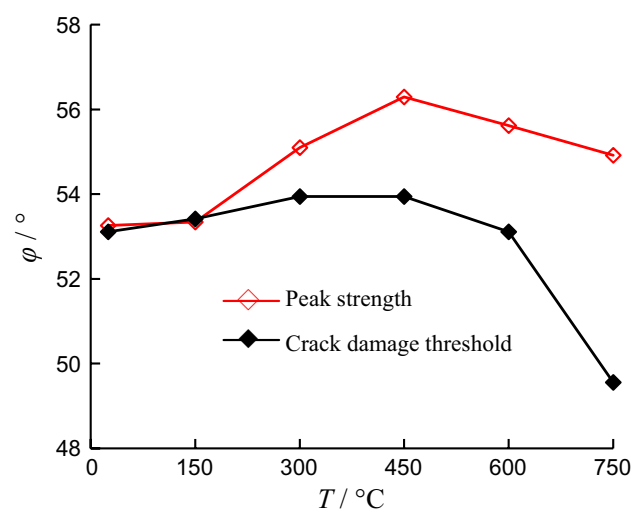
Fig. 24 Effect of temperature on internal friction angle of granite obtained by peak strength and crack damage threshold

ductivity of granite as a function of the temperature. The experimental results show that the mass, P-wave velocity, and thermal conductivity of the granite decrease but the volume increases with increasing temperature. High temperature also has a notable effect on the permeability evolution behaviour. The permeability decreases with increasing axial and confining pressure, while the confining pressure has a larger influence than the axial stress in the range of 10–50 MPa. A theoretical model was constructed to analyse the effect of the volumetric stress on the permeability coefficient of granite, which agrees very well with the experimental results. The initial and ultimate permeabilities increase exponentially with increasing temperature.

2. The triaxial stress–strain curve of granite after high-temperature treatment can be divided into five stages: (I) initial pore and fissure closure stage; (II) elastic deformation stage; (III) plastic deformation stage; (IV) post-peak failure stage, and (V) residual strength stage. The range of stage I gradually decreases with increasing confining pressure but this stage becomes more apparent with increasing temperature. The average slope between the stress and the axial strain (stage II) of granite increases nonlinearly with increasing confining pressure, but the increasing rate is more sensitive to the confining pressure under suffering higher temperature treatment. With increasing temperature and confining pressure, the stress drop of granite during stage III becomes less and less obvious. During stage IV, the post-stress reduces slowly with increasing deformation. However, after high temperature and at high confining pressure, the post-peak stress reduces significantly due to the formation of transgranular cracks. To some extent, the confining pressure decreases the effect of the high temperature pre-treatment on the stress–strain curve.

3. The effect of high temperature on the triaxial deformation and AE behaviour of granite was investigated. Under uniaxial compression, the Young's modulus first increases, then decreases, and finally remains relatively constant with increasing temperature; whereas the variation sensitivity reduces with increasing confining pressure. At $T \leq 300$ °C, stress drops can be observed before the peak strength is reached, which correspond to a significant AE event and are caused by the formation of multiple splitting tensile cracks in the loading direction. At $T \geq 450$ °C, AE can be observed once a minor stress is applied because the failure mode is controlled by thermally induced cracks. However, under triaxial compression, the temperature has little effect on the AE characteristics. The granite fails along the shear fracture plane, which widens with increasing confining pressure. However, at $T \geq 600$ °C, intragranular cracks are more easily generated and the stress quickly decreases after the peak strength is reached. The shear plane is smoother at higher confining pressure.

4. With increasing temperature, the peak strength and crack damage threshold first remain relatively constant, then decrease, and finally are constant between 600 and 750 °C. This can be explained as follows: Mica is oxidised at 400 °C, the α–β phase transformation of quartz occurs at 573 °C, and macroscopic cracks are initiated at 600 °C. Because the thermal stress is released, the propagation of macroscopic cracks becomes more difficult. The peak strength and crack damage threshold of granite nonlinearly increases with the confining pressure. The mechanism based on which the high temperature affects the triaxial strength parameters of granite is discussed.

At $T \leq 300$ °C, thermally induced cracks are not notable and the temperature has a limited effect on the behaviour of granite. At 450 °C $\leq T \leq 600$ °C, thermally induced cracks can be observed and the temperature has a significant effect on the strength behaviour of granite. Because thermal stress is released by the formation of thermal macrocracks, the continuous increase in the temperature has a limited effect on the strength behaviour of granite, even at the maximum temperature of 750 °C.

Compliance with Ethical Standards

Conflict of interest The authors declare no conflict of interests.

References

Chaki S, Takarli M, Agbodjan WP (2008) Influence of thermal damage on physical properties of a granite rock: porosity, permeability and ultrasonic wave evolutions. Constr Build Mater 22(7):1456–1461

Chen S, Yang C, Wang G (2017a) Evolution of thermal damage and permeability of Beishan granite. Appl Therm Eng 110:1533–1542

Chen YL, Wang SR, Ni J, Azzam R, Fernandez-Steeger TM (2017b) An experimental study of the mechanical properties of granite after high temperature exposure based on mineral characteristics. Eng Geol 220:234–242

Chen G, Wang J, Li J, Li T, Zhang H (2018) Influence of temperature on crack initiation and propagation in granite. Int J Geomech 18(8):04018094

Consenza P, Ghoreychi M (1999) Effects of very low permeability on the long-term evolution of a storage cavern in rock salt. Int J Rock Mech Min Sci 36:527–533

Davy CA, Skoczylas F, Barnichon JD, Lebon P (2007) Permeability of macro-cracked argillite under confinement: gas and water testing. Phys Chem Earth 32:667–668

Fairhurst CE, Hudson JA (1999) Draft ISRM suggested method for the complete stress–strain curve for intact rock in uniaxial compression. Int J Rock Mech Min Sci 36(3):279–289

Fan LF, Gao JW, Wu ZJ, Yang SQ, Ma GW (2018) An investigation of thermal effects on micro-properties of granite by X-ray CT technique. Appl Therm Eng 140:505–519

Gautam PK, Verma AK, Sharma P, Singh TN (2018) Evolution of thermal damage threshold of Jalore granite. Rock Mech Rock Eng 51(9):2949–2956

Griffiths L, Heap MJ, Baud P, Schmittbuhl J (2017) Quantification of microcrack characteristics and implications for stiffness and strength of granite. Int J Rock Mech Min Sci 100:138–150

Guo LL, Zhang YB, Zhang YJ et al (2018) Experimental investigation of granite properties under different temperatures and pressures and numerical analysis of damage effect in enhanced geothermal system. Renew Energy 126:107–125

Gustafsson SE (1991) Transient plane source techniques for thermal conductivity and thermal diffusivity measurements of solid materials. Rev Sci Instrum 62:797–804

Heap MJ, Baud P, Meredith PG, Bell AF, Main IG (2009) Time-dependent brittle creep in Darley Dale sandstone. J Geophys Res. https://doi.org/10.1029/2008JB006212

Hoek E (1990) Estimating Mohr–Coulomb friction and cohesion values from the Hoek–Brown failure criterion. Int J Rock Mech Min Sci Geomech Abstr 12:227–229

Hoek E, Brown ET (1980) Underground excavation in rock. Institution of Mining and Metallurgy, London

Hu J, Sun Q, Pan X (2018) Variation of mechanical properties of granite after high-temperature treatment. Arab J Geosci 11(2):43

Huang YH, Yang SQ, Tian WL, Zhao J, Ma D, Zhang CS (2017) Physical and mechanical behavior of granite containing pre-existing holes after high temperature treatment. Arch Civ Mech Eng 17(4):912–925

Jiang G, Zuo J, Li L, Ma T, Wei X (2018) The evolution of cracks in Maluanshan granite subjected to different temperature processing. Rock Mech Rock Eng 51(6):1683–1695

Log T, Gustafsson SE (1995) Transient plane source (TPS) technique for measuring thermal transport properties of building materials. Fire Mater 19:43–49

Mckee CR, Bumb AC, Koenig RA (1988) Stress-dependent permeability and porosity of coal and other geologic formations. SPE Form Eval 3(01):81–91

Mitchell EK, Fialko Y, Brown KM (2013) Temperature dependence of frictional healing of Westerly granite: experimental observations and numerical simulations. Geochem Geophys Geosyst 14(3):567–582

Nasseri MHB, Schubnel A, Young RP (2007) Coupled evolutions of fracture toughness and elastic wave velocities at high crack density in thermally treated Westerly granite. Int J Rock Mech Min Sci 44(4):601–616

Ranjith PG, Viete DR, Chen BJ, Perera MS (2012) Transformation plasticity and the effect of temperature on the mechanical behaviour of Hawkesbury sandstone at atmospheric pressure. Eng Geol 151:120–127

Shao S, Ranjith PG, Wasantha PLP, Chen BK (2015) Experimental and numerical studies on the mechanical behaviour of Australian Strathbogie granite at high temperatures: an application to geothermal energy. Geothermics 54:96–108

Sun SH (1987) The choice of calculating scheme of mica formula. Acta Petrol Sin 4:72–82 **(in Chinese)**

Sun Q, Zhang W, Xue L, Zhang Z, Su T (2015) Thermal damage pattern and thresholds of granite. Environ Earth Sci 74(3):2341–2349

Sundberg J, Hellström G (2009) Inverse modelling of thermal conductivity from temperature measurements at the Prototype Repository, Äspö HRL. Int J Rock Mech Min Sci 46(6):1029–1041

Urquhart A, Bauer S (2015) Experimental determination of single-crystal halite thermal conductivity, diffusivity and specific heat from 75 to 300 °C. Int J Rock Mech Min Sci 78:350–352

Wang HF, Bonner BP, Carlson SR, Kowallis BJ, Heard HC (1989) Thermal stress cracking in granite. J Geophys Res Solid Earth 94(B2):1745–1758

Wang Z, He A, Shi G, Mei G (2017) Temperature effect on AE energy characteristics and damage mechanical behaviors of granite. Int J Geomech 18(3):04017163

Williams H, Turner FJ, Gilbert CM (1954) Petrography. Freeman, San Francisco

Wong TF, David C, Zhu W (1997) The transition from brittle faulting to cataclastic flow in porous sandstones. Mech Deform J Geophys Res 102(B2):3009–3025

Xu P, Yang SQ (2019) Influence of stress and high-temperature treatment on the permeability evolution behavior of sandstone. Acta Mech Sin 35(2):419–432

Xu XL, Zhang ZZ (2018) Acoustic emission and damage characteristics of granite subjected to high temperature. Adv Mater Sci Eng. https://doi.org/10.1155/2018/8149870

Yang SQ, Ranjith PG, Huang YH, Yin PF, Jing HW, Gui YL, Yu QL (2015) Experimental investigation on mechanical damage characteristics of sandstone under triaxial cyclic loading. Geophys J Int 201:662–682

Yang SQ, Ranjith PG, Jing HW, Tian WL, Ju Y (2017) An experimental investigation on thermal damage and failure mechanical behavior of granite after exposure to different high temperature treatments. Geothermics 65:180–197

Yang SQ, Tian WL, Huang YH (2018) Failure mechanical behavior of pre-holed granite specimens after elevated temperature treatment by particle flow code. Geothermics 72:124–137

Yang SQ, Huang YH, Tian WL, Yin PF, Jing HW (2019) Effect of high temperature on deformation failure behavior of granite specimen containing a single fissure under uniaxial compression. Rock Mech Rock Eng. https://doi.org/10.1007/s00603-018-1725-5

Yin T, Li X, Cao W, Xia K (2015) Effects of thermal treatment on tensile strength of Laurentian granite using Brazilian test. Rock Mech Rock Eng 48(6):2213–2223

Zhang F, Zhao J, Hu D, Skoczylas F, Shao J (2018) Laboratory investigation on physical and mechanical properties of granite after heating and water-cooling treatment. Rock Mech Rock Eng 51(3):677–694

Zhao XG, Cai M, Wang J, Li PF (2015) Strength comparison between cylindrical and prism specimens of Beishan granite under uniaxial compression. Int J Rock Mech Min Sci 76:10–17

Zhao XG, Wang J, Chen F, Li PF, Ma LK, Xie JL, Liu YM (2016) Experimental investigations on the thermal conductivity characteristics of Beishan granitic rocks for China's HLW disposal. Tectonophysics 683:124–137

Zhao Y, Feng Z, Zhao Y, Wan Z (2017) Experimental investigation on thermal cracking, permeability under HTHP and application for geothermal mining of HDR. Energy 132:305–314

Zhao XG, Zhao Z, Guo Z et al (2018) Influence of thermal treatment on the thermal conductivity of Beishan granite. Rock Mech Rock Eng 51(7):1–20

Zhu TT, Jing HW, Su HJ, Yin Q, Du MR, Han GS (2016) Physical and mechanical properties of sandstone containing a single fissure after exposure to high temperatures. Int J Min Sci Technol 26(2):319–325